Strength and Ductility of Corner Materials in Cold-Formed Stainless Steel Sections

W. M. Quach*, and P. Qiu
Department of Civil and Environmental Engineering, University of Macau, Macau, China

ABSTRACT
The cold work from the manufacturing process of cold-formed steel members can enhance the strength but reduce the ductility of materials. Due to the high cost of stainless steels, it is desirable to utilize this enhanced strength and avoid the early fracture in cold-formed stainless steel members. The paper is concerned with the prediction of the enhanced stress-strain behaviour and reduced ductility of corner materials in cold-formed stainless steel sections. The enhanced strength of corner materials has been traditionally determined using empirical models. However, most of these empirical models are only able to predict the enhanced 0.2% proof strength, but are neither capable of predicting the enhanced ultimate strength nor able to determine the reduced ductility. This paper first presents a modified weighted-average method for predicting the post-ultimate stress-strain behaviour and the fracture strain for stainless steels. An advanced numerical approach is next presented for predicting the full-range stress-strain behaviour of corner materials in cold-formed stainless steel sections, in which the modified weighted-average method is incorporated. The accuracy of this approach is demonstrated by comparing its predictions with test results. The proposed approach is generally applicable to cold-worked materials for predicting their enhanced strength, reduced ductility and full-range stress-strain behaviour. The proposed method and numerical results can explain why and how the ultimate strength of cold-formed steels can be increased and how the post-ultimate stress-strain behaviour can be utilized through cold working.

KEYWORDS
Stainless steels, corner, cold work, strength enhancement, reduced ductility, post-ultimate stress-strain behaviour.

HIGHLIGHTS
- A new method for predicting the post-ultimate stress-strain behaviour of metals
- Theoretical prediction of the strain at the onset of localized necking
- FE predictions of the enhanced strength and reduced ductility of corner materials
- Utilize post-ultimate stress-strain behaviour of stainless steels through cold work

1. INTRODUCTION

Cold-formed steel members are usually manufactured by either roll forming or press braking. These forming processes can induce cold work in members and significantly changes the mechanical behaviour of the material, including an increase in the strength and a reduction in the ductility. A large strength enhancement and a great reduction of ductility are usually found in the material in the corners (or the so-called corner material) of cold-formed sections. The strength enhancement in the corner material of cold-formed carbon steel and stainless steel sections has been investigated by many researchers [1–7]. The earliest experimental work for determining the corner properties of cold-formed carbon steel sections was done by Karren [1]. He found that the method of forming had only little influence on the mechanical properties of corners, and proposed a semi-empirical equation for predicting the yield strength of corners in carbon steel sections, which is a function of the corner radius and the mechanical properties of virgin steel sheets.

Due to the great extent of strain hardening of stainless steel alloys, the strength enhancement in corners of cold-formed stainless steel sections has interested many researchers. Based on Karren's methodology [1], some empirical models for the prediction of the corner strength of stainless steel sections were proposed by different researchers [3,4,6,7]. Due to the high cost of stainless steels, it is desirable to not only utilize the enhanced strength but also avoid the early fracture arising from cold forming. On the other hand, the stress-strain relationship of corner materials would be needed for the nonlinear finite element (FE) analysis of the buckling behaviour of cold-formed stainless steel members but less information on this relationship is available as addressed by Greiner and Kettler [8]. However, most of these existing empirical models [3,4,7] for stainless steel corners are only applicable to the prediction of the enhanced 0.2% proof stress, but are neither capable of predicting the enhanced ultimate strength nor able to predict the reduced ductility and full-range stress-strain behaviour of corner materials. The empirical model proposed by Ashraf et al. [6] is capable of predicting both the enhanced 0.2% proof stress and the enhanced ultimate strength of corner materials, but has not tackled the issue of the reduced ductility of corner materials in cold-formed stainless steel sections.

Accurate theoretical predictions of a complete stress-strain relationship of corner materials up to the fracture strain are needed for the advanced FE analysis of cold-formed stainless steel structures and are not yet available. Nevertheless, a limited amount of effort has been made in the theoretical prediction of the enhanced 0.2% proof stress of stainless steel cold-worked materials

© W.M. Quach & P. Qiu, University of Macau

[9]. A research team [9] at the University of Liège proposed a theory-based formula for the prediction of the enhanced 0.2% proof stress of stainless steel corner materials. In the theory-based formula [9], the enhanced 0.2% proof stress is calculated by considering a plastic strain offset of 0.2% plus the corner bending strain from the nominal stress-strain relationship of virgin stainless steel sheets. However, their method cannot be used for the prediction of the enhanced ultimate strength in corners as the maximum enhanced strength obtained from the formula is limited by the nominal ultimate strength of virgin sheets. Although accurate predictions of the full-range stress-strain relationship of corner materials for strains up to fracture are not yet available as mentioned earlier, some theoretical and numerical studies [10–15] have been attempted to predict the stress-strain relationship of flat metal strips up to the fracture strain. However, in these existing studies, fracture strains were usually determined experimentally or using assumed values.

This paper is concerned with an accurate prediction of the enhanced stress-strain behaviour and reduced ductility of the corner material in cold-formed stainless steel sections by presenting an advanced numerical approach for the simulation of corner coupon tests. In the present paper, an analytical method, namely the modified weighted-average method, is first presented for predicting the full-range stress-strain behaviour of flat virgin strips up to the fracture strain. In this method, the fracture strain of virgin sheets can be determined analytically. An advanced numerical approach is then presented for predicting the reduced ductility and enhanced stress-strain behaviour of corner materials in cold-formed stainless steel sections, in which the modified weighted-average method is incorporated. In this approach, the effect of cold work from forming on the stress-strain behaviour of the corner material is taken into account accurately. The proposed approach can overcome the aforementioned difficulties and limitations encountered by existing empirical models [3–7]. The accuracy of the proposed approach is demonstrated by comparing its predictions with test results.

2. SCOPE OF WORK AND TERMINOLOGY

As the present paper deals with the theoretical and numerical modelling of the mechanical behaviour of thin-walled stainless steels, the failure process of metal strips in tension tests is first introduced in this section. In a uniaxial tension test of a flat metal strip, plastic instability and flow localization occur at the maximum load (i.e., the nominal ultimate stress) and the so-called diffuse necking starts (such as point U in Fig. 1) [12]. The diffuse necking occurs along the width direction and spreads over a length of the order of the width. At the end of diffuse necking, localized necking starts (such as point L in Fig. 1) and occurs with a through thickness neck over a narrow band of the order of the sheet thickness, inclined at an angle to the specimen axis. The localized necking eventually leads to final fracture (such as point F in Fig. 1). Fig. 1 shows the typical nominal stress-strain curve of a flat tension specimen with a rectangular cross section. As shown in Fig. 1, the process from the onset of localized necking to fracture (such as the loading path L-F in Fig. 1) is often a very short and rapid process [12]. This two-stage necking process is illustrated in Fig. 2. The same necking process can also be found in the tension test of corner specimens in an experimental study reported in the next section. This can be seen from Fig. 3 which shows the typical deformed shapes of a flat specimen and a corner specimen respectively after fracture.

To verity the advanced numerical approach for capturing the aforementioned necking process, an experimental study on the mechanical properties of both virgin and corner materials of cold-formed stainless steel sections has been carried out and is first introduced in Section 3. The mechanical properties of flat sheets can be considered to represent the properties of virgin materials. In order to predict the enhanced strength and reduced ductility of corner materials in cold-formed stainless steel sections numerically, a full-range stress-strain relationship of stainless steel sheets for strains up to fracture is required. The stress-strain relationship of stainless steels before diffuse necking can be easily defined by either laboratory testing or existing stress-strain models [16,17] with high accuracy, but the method for determining the stress-strain relationship for strains after diffuse necking are not well defined. Therefore, the stress-strain relationship of flat sheets after diffuse necking (simply referred to as the post-ultimate stress-strain relationship hereafter) should be accurately defined first. To establish this relationship up to the fracture strain of flat sheets, a modified weighted-average method has been proposed as a part of the present study and is presented in Section 4. In Section 5, the advanced numerical approach is presented for predicting the enhanced strength, reduced ductility, and full-range stress-strain behaviour of corner materials in cold-formed stainless steel sections, in which the modified weighted-average method is incorporated. The accuracy of this numerical approach is demonstrated in Section 6 by comparing its predictions with test results. Predictions of corner enhanced strengths obtained from the advanced numerical approach are also compared with predictions given by existing empirical models. This comparison is also presented in Section 6.

Before proceeding further, the terminology adopted in this paper in referring to stresses in various directions should be noted first. The length direction of a stainless steel sheet is referred to as the longitudinal direction (z direction) and the width direction of the sheet is referred to as the transverse direction (x direction), while the direction normal to the sheet is referred to as the through-thickness direction (y direction). The longitudinal direction of a stainless steel sheet remains the axial load direction of the corner specimen produced from the sheet.

3. EXPERIMENTAL STUDY

In the experimental study, two batches of tension coupon tests on both flat and corner specimens were performed. All specimens were prepared and tested according to specifications in AS 1391:1991 [18]. In each batch, two stainless steel grades including grades 304 and 316L were considered and were provided in 1220mm by 2200mm sheets with nominal thicknesses t of 2 mm. Both flat and corner specimens were cut and prepared from each stainless steel sheet, and two different inner corner radii r_i were considered with their nominal values being r_i = 4 mm and 6 mm respectively. To measure material anisotropy characteristics, flat specimens were cut along the longitudinal (L), transverse (T), and 45° diagonal (D) directions respectively. All specimens were taken from positions located one quarter of the sheet width from both edges. To prepare corner specimens, smaller stainless steel strips were cut first from the 1220mm by 2200mm sheets, and then press-braked into angle sections. Each corner specimen was fabricated from each of these press-braked angles, and only the corner region was remained within the parallel length of the specimen. The fold line of each angle coincides with the longitudinal direction of the sheet.

Electrical strain gauges were placed on two opposite faces at the mid-length of each specimen (including flat and corner specimens) to measure the initial stress-strain data up to strains of about 1~3%, and the average of two strain readings was taken. Extensometers capable of 100% tensile strain measurement were used to measure the full-range stress-strain behaviour up to fracture for each flat or corner specimen. A gauge length of 50 mm was used for both flat and corner specimens, unless otherwise stated.

In the present study, two types of corner coupon testing methods have been used: (1) single corner coupon test (SC) and (2) twin corner coupon test (TC) (see Fig. 4). In the single corner coupon test (see Fig. 4(a)), the position of each specimen was adjusted and aligned such that the loading axis passed through the centroid of the corner cross section, and pin supports were provided at both the top and the bottom of the specimen to reduce the bending effect due to the singly symmetrical pattern of the cross section. As shown in Fig. 5, the difference between two initial stress-strain curves, respectively, measured by the strain gauges on two opposite faces of each single corner coupon are very small and thus the bending effect on the measured stress-strain curve can be considered to be negligible. In the twin corner coupon test, corner coupons of the same corner radius and dimensions were tested in pair, and the testing was achieved by symmetrically gripping the ends of the twin coupons around steel bars (see Fig. 4(b)). There were only two extensometers available for 100% tensile strain measurement: one with 50-mm gauge length and another with 25-mm gauge length. Therefore, in the twin corner coupon test, one of the twin coupons was measured using the extensometer of 50-mm gauge length while the another corner coupon in the pair was measured using the extensometer of 25-mm gauge length.

Totally 16 single corner coupon tests and 8 twin corner coupon tests were carried out. All specimens in the first batch were tested at a displacement rate of 0.2mm/min, and specimens in the second batch were tested at a displacement rate of 0.1mm/min. In the first batch, one single corner test and one twin corner coupon test were performed for each stainless steel grade (i.e., grades 304 and 316L) and each nominal inner corner radius (i.e., r_i = 4 mm, 6 mm). In the second batch, triplicate tests were performed for each stainless steel grade and each inner corner radius using the single corner coupon testing method, while duplicate tests of corners with r_i = 6 mm were performed for each grade using the twin corner coupon testing method.

The test specimens were labelled such that the batch of specimens, stainless steel grade, type of the specimen, testing method, nominal inner corner radius and thickness could be identified from the label. For example, in the label "SB-316L-SCr4t2-2", the first two letters "SB" indicate that the specimen belongs to the second batch, the notation "316L" is referred to as the grade 316L, the following letters "SC" indicates the single corner coupon test, and the notation "r4t2" indicates a specimen with the 4-mm nominal inner corner radius and 2-mm nominal thickness. If a test was repeated, then "-1", "-2" and "-3" indicate the first, second and third repeated tests respectively.

Table 1 summarizes measured mechanical properties of virgin stainless steel sheets, including the initial elastic modulus E_0, the strain-hardening exponent n, the nominal 0.2% proof stress $\sigma_{0.2,v}$, the nominal ultimate strength $\sigma_{u,v}$ and the nominal total strain $\varepsilon_{u,v}$ at $\sigma_{u,v}$ of virgin sheets for the longitudinal direction. Other measured mechanical properties of stainless steel sheets are presented in Section 5. Table 2 summarizes test results of corner materials, including the nominal 0.2% proof stress $\sigma_{0.2,c}$, the nominal ultimate strength $\sigma_{u,c}$ and the percentage elongation $\varepsilon_{50,c}$ over a 50-mm gauge length of corner specimens. The measured $\sigma_{0.2,c}/\sigma_{0.2,v}$ and $\sigma_{u,c}/\sigma_{u,v}$ ratios are also presented in the table, and can be used to indicate the strength enhancement in corners. The $\sigma_{0.2,c}/\sigma_{0.2,v}$ ratio varies from 1.35 to 1.97, while the $\sigma_{u,c}/\sigma_{u,v}$ ratio varies from 1.04 to 1.21. It can be seen that the 0.2% proof stress and ultimate strength of materials in corners can be significantly

increased by maximum amounts of 97% and 21% respectively as a result of cold working. Fig. 6 shows the comparison of measured stress-strain curves between the corner material and virgin material, which demonstrates the significant strength enhancement and ductility reduction of the corner material arising from cold working.

4. POST-ULTIMATE STRESS-STRAIN BEHAVIOUR OF VIRGIN SHEETS

4.1 General

The strain-hardening behaviour of an isotropic metal is described by its true stress-true plastic strain relationship. A weighted-average method was proposed by Ling [11], to model the true stress-true plastic strain relationship of flat metal strips after diffuse necking. However, the method [11] is only applicable to isotropic metals and is not capable of the prediction of the fracture strain or the strain at the onset of localized necking, which needs to be determined experimentally. In order to take account of the effect of material anisotropy of stainless steel alloys and facilitate the FE simulation of the stress-strain behaviour of corner materials up to the fracture strain, the weighted-average method [11] has been modified in the present study and is presented in the next two subsections.

4.2 Weighted-average method

The weighted-average method [11] is summarized in this subsection for determining the tensile true stress-true plastic strain relationship of flat strips after diffuse necking.

According to Considère's criterion [19], the condition at the onset of diffuse necking of a flat strip under uniaxial tension is given by Eq. (1):

$$\sigma_t = \sigma_{t,u} \quad \text{and} \quad \frac{d\sigma_t}{d\varepsilon_{tp}} = \sigma_{t,u} \quad \text{at} \quad \varepsilon_{tp} = \varepsilon_{tp,u} \tag{1}$$

where σ_t and ε_{tp} are the true stress and the true plastic strain respectively, and $\sigma_{t,u}$ and $\varepsilon_{tp,u}$ are the true stress at the onset of diffuse necking and the corresponding true plastic strain respectively. The values of $\sigma_{t,u}$ and $\varepsilon_{tp,u}$ are those corresponding to the nominal ultimate stress $\sigma_{n,u}$ (i.e., the maximum nominal stress at point U in Fig. 1) determined from the uniaxial tension test. The true stress and true plastic strain before diffuse necking can be found from the nominal stress σ_n and the nominal strain ε_n measured in the tension test using the following equation [20]:

$$\sigma_t = \sigma_n\left(1+\varepsilon_n\right) \quad \text{and} \quad \varepsilon_{tp} = \ln\left(1+\varepsilon_n\right) - \frac{\sigma_t}{E_o} \ . \tag{2}$$

If a power-law function $\sigma_t = K\varepsilon_{tp}^{\ n_s}$ (in which K and n_s are constants) is used to extrapolate the true stress-true plastic strain relationship beyond diffuse necking, the onset of diffuse necking should be reserved and constants K and n_s can be determined from Eq. (1) as

$$K = \frac{\sigma_{t,u}}{\varepsilon_{tp,u}^{\ \varepsilon_{tp,u}}} \quad \text{and} \quad n_s = \varepsilon_{tp,u} \ . \tag{3}$$

Thus, the power-law relationship becomes

$$\sigma_t = \sigma_{t,u}\left(\frac{\varepsilon_{tp}}{\varepsilon_{tp,u}}\right)^{\varepsilon_{tp,u}} \ . \tag{4}$$

If a linear function $\sigma_t = a_0 + a_1\varepsilon_{tp}$ (in which a_0 and a_1 are constants) is used to describe the true stress-true plastic strain relationship after diffuse necking, constants a_0 and a_1 can be determined from Eq. (1) as

$$a_0 = \sigma_{t,u}(1-\varepsilon_{tp,u}) \text{ and } a_1 = \sigma_{t,u} \ . \tag{5}$$

Thus, the linear relationship becomes

$$\sigma_t = \sigma_{t,u}(1+\varepsilon_{tp}-\varepsilon_{tp,u}) \ . \tag{6}$$

As observed by Ling [11], the power-law extrapolation appears to underestimate true stresses while the linear extrapolation generally overestimates true stresses. Thus, as suggested by Ling [11], a better approximation of the true stress-true plastic strain relationship of flat metal strips for strains beyond the onset of diffuse necking can be expressed as the weighted average of these two bounds through Eq. (7):

$$\sigma_t = \sigma_{t,u}\left[w(1+\varepsilon_{tp}-\varepsilon_{tp,u}) + (1-w)\left(\frac{\varepsilon_{tp}}{\varepsilon_{tp,u}}\right)^{\varepsilon_{tp,u}} \right] \tag{7}$$

in which w is an unknown weight constant with $0 \le w \le 1$, and the conditions $w = 0$ and $w = 1$ represent a power-law extrapolation (lower bound) and a linear extrapolation (upper bound) respectively.

To determine the unknown weight constant w, the measured nominal stress-strain curve can be treated as the target and the weight constant is varied in a FE model until the predicted nominal stress-strain curve immediately prior to fracture agrees closely with the measured stress-strain curve. The end point of the resulting true stress-true plastic strain curve represents the true plastic strain at fracture which cannot be determined analytically and needs to be determined experimentally in Ling's method [11]. To overcome this limitation of the weighted-average method [11] and take account of the effect of material anisotropy of stainless steels as mentioned earlier, this method has been modified and the modification is presented in the next subsection.

4.3 Modified weighted-average method

A flat strip cut along the longitudinal direction of an anisotropic metal sheet is considered. During the localized necking of the flat strip under uniaxial tension, the neck cross-sectional area undergoes a change due to a decrease dt in the thickness t only with no change in the width. Thus, the instability condition for localized necking is given by Eq. (8) [21,22]:

$$\frac{d\sigma_z}{\sigma_z} = -\frac{dt}{t} = -d\varepsilon_{py} \tag{8}$$

where σ_z is the principal stresses in the longitudinal (z) direction, $d\varepsilon_{py}$ is the principal plastic strain increment along the through-thickness (y) direction.

According to the flow rule, plastic strain increments for anisotropic materials are given by

$$\begin{Bmatrix} d\varepsilon_{px} \\ d\varepsilon_{py} \\ d\varepsilon_{pz} \end{Bmatrix} = d\lambda \begin{Bmatrix} H(\sigma_x-\sigma_y)+G(\sigma_x-\sigma_z) \\ F(\sigma_y-\sigma_z)+H(\sigma_y-\sigma_x) \\ G(\sigma_z-\sigma_x)+F(\sigma_z-\sigma_y) \end{Bmatrix} \tag{9}$$

where $d\lambda$ is a positive scalar representing the magnitude of the plastic strain increment vector; σ_x and σ_y are the principal stresses in the x and y directions; $d\varepsilon_{px}$ and $d\varepsilon_{pz}$ are the principal plastic strain increments along the x and z directions respectively; and F, G and H are anisotropy parameters. These anisotropy parameters are defined by Eq. (10) [23]:

$$F = \frac{1}{2}\left[\frac{1}{\sigma_{0N}^2} + \frac{1}{\sigma_{0L}^2} - \frac{1}{\sigma_{0T}^2} \right] \tag{10a}$$

$$G = \frac{1}{2}\left[\frac{1}{\sigma_{0T}^2} + \frac{1}{\sigma_{0L}^2} - \frac{1}{\sigma_{0N}^2}\right] \tag{10b}$$

$$H = \frac{1}{2}\left[\frac{1}{\sigma_{0T}^2} + \frac{1}{\sigma_{0N}^2} - \frac{1}{\sigma_{0L}^2}\right] \tag{10c}$$

in which σ_{0L}, σ_{0T} and σ_{0N} are the initial yield stresses (taken as the 0.2% proof stresses) in the longitudinal (z), transverse (x) and through-thickness (y) directions respectively. The through-thickness 0.2% proof stress σ_{0N} is approximated by the diagonal 0.2% proof stress σ_{0D} (i.e. $\sigma_{0N} \cong \sigma_{0D}$) as suggested by Quach et al. [24,25].

For the state of uniaxial stresses in the longitudinal (z) direction, $\sigma_x = 0$, $\sigma_y = 0$, and $\sigma_z = \sigma_{yL}$ (where σ_{yL} is the instantaneous yield stress in the longitudinal direction). The ratio between $d\varepsilon_{py}$ and $d\varepsilon_{pz}$ can be obtained from Eq. (9) as

$$\frac{d\varepsilon_{py}}{d\varepsilon_{pz}} = \frac{-F}{G+F} \tag{11}$$

By substituting Eq. (11) into Eq. (8), the condition for the localized necking of anisotropic materials can be obtained as

$$\frac{d\sigma_z}{\sigma_z} = -d\varepsilon_{py} = \frac{F}{G+F}d\varepsilon_{pz} \ . \tag{12}$$

In Eq. (12), σ_z and ε_{pz} represent the true stress σ_t and the true plastic strain ε_{tp} respectively, obtained from the uniaxial tension test of the longitudinal flat specimen. Thus, Eq. (12) can be re-written as

$$\frac{d\sigma_t}{d\varepsilon_{tp}} = \frac{\sigma_t}{1+R} \tag{13}$$

where $R = G/F$.

For isotropic materials, $R = 1$ (i.e., $G = F$) and Eq. (13) becomes

$$\frac{d\sigma_t}{d\varepsilon_{tp}} = \frac{\sigma_t}{2} \tag{14}$$

which gives the condition for the localized necking of isotropic materials.

According to the weighted-average method [11], the true stress-true plastic strain relationship $\sigma_t(\varepsilon_{tp})$ after diffuse necking is expressed as the weighted average of the power-law extrapolation and the linear extrapolation (see Eq. (7)). Substituting Eq. (7) and its differentiation into Eq. (13) yields Eq. (15) which represents a condition at the onset of localized necking:

$$\left(\frac{w}{1+R}\right)\left(1+\varepsilon_{tp}-\varepsilon_{tp,u}\right)+\left(\frac{1-w}{1+R}\right)\left(\frac{\varepsilon_{tp}}{\varepsilon_{tp,u}}\right)^{\varepsilon_{tp,u}} - (1-w)\left(\frac{\varepsilon_{tp}}{\varepsilon_{tp,u}}\right)^{\varepsilon_{tp,u}-1} - w = 0 \quad \text{at } \varepsilon_{tp} = \varepsilon_{tp,f} \tag{15}$$

where $\varepsilon_{tp,f}$ is the true plastic strain at the onset of localized necking. For each trial *w*, the true plastic strain $\varepsilon_{tp,f}$ at the onset of localized necking can be obtained from Eq. (15). As the process from the onset of localized necking to fracture is often a

rapid process [12], the strain increment induced by localized necking is ignored in the present study. Therefore, the true plastic strain at fracture is approximated by the true plastic strain $\varepsilon_{tp,f}$ at the onset of localized necking hereafter.

It is worth noting that the trial true stress-true plastic strain relationship should be converted to the equivalent stress-equivalent plastic strain relationship for describing the strain-hardening behaviour of anisotropic metals through Eq. (16) [23]:

$$\overline{\sigma} = \sqrt{\frac{3}{2}\left(\frac{F+G}{F+G+H}\right)}\sigma_t \quad \text{and} \quad \overline{\varepsilon}_p = \sqrt{\frac{2}{3}\left(\frac{F+G+H}{F+G}\right)}\varepsilon_{tp} \ . \tag{16}$$

Thus, the equivalent plastic strain at fracture can be approximated by the equivalent plastic strain at the onset of localized necking, and is obtained from Eq. (16) as

$$\overline{\varepsilon}_{p,f} = \sqrt{\frac{2}{3}\left(\frac{F+G+H}{F+G}\right)}\varepsilon_{tp,f} \ . \tag{17}$$

To determine the unknown weight constant w and the corresponding equivalent plastic strain $\overline{\varepsilon}_{p,f}$ at fracture, an approach similar to Ling's method [11] is followed. The resulting equivalent stress-equivalent plastic strain relationship up to fracture is obtained after a successful trial of w.

For materials with w = 0, Eq. (15) reduces to Eq. (18) for the prediction of the true plastic strain $\varepsilon_{tp,f}$ at fracture:

$$\varepsilon_{tp,f} = (1+R)\varepsilon_{tp,u} \ . \tag{18}$$

For materials with w = 1.0, Eq. (15) reduces to Eq. (19) for $\varepsilon_{tp,f}$:

$$\varepsilon_{tp,f} = R + \varepsilon_{tp,u} \ . \tag{19}$$

5. NUMERICAL PREDICTION OF THE MECHANICAL BEHAVIOUR FOR CORNER MATERIALS

5.1 Numerical analysis procedure

The advanced numerical approach for modelling the mechanical behaviour of corner materials was implemented using the FE package ABAQUS [26]. The three stages of the advanced approach are summarized below. Further details of the analysis procedure are given later in the paper.

5.1.1 Stage I: The stress-strain relationship of virgin sheets up to fracture

In the first stage, the stress-strain behaviour of the virgin material in the longitudinal direction (i.e., the loading direction) is determined for strains up to the fracture strain which can be closely approximated by the strain at the end of diffuse necking. The modelling of material nonlinearity in ABAQUS requires the definition of a true stress-true plastic strain relationship for isotropic metals and an equivalent stress-equivalent plastic strain relationship for anisotropic metals as input data.

To achieve this task, a compound true stress-true plastic strain relationship of the virgin material in the longitudinal direction is constructed to cover two ranges of strains up to the fracture strain: (i) the true stress-true plastic strain relationship for stresses up to the onset of diffuse necking is found first from the measured stress-strain data up to the nominal ultimate stress (such as the loading path O-U in Fig. 1) using Eq. (2); and (ii) it is then determined for a range of strains throughout the process of diffuse necking using the modified weighted-average method together with a trial weight constant w as presented in the preceding section (see Eqs. (7) and (15)). To determine the unknown weight constant w and the corresponding fracture strain in the modified weighted-average method, a FE simulation of the flat tension coupon test of the virgin material is carried out for each trial value of w. Once the compound true stress-true plastic strain relationship in the longitudinal direction is obtained after a successful trial of w (i.e., the FE predicted nominal stress-strain curve agrees with the measured stress-strain curve), the "compound" equivalent stress-equivalent plastic strain relationship for anisotropic metals can be established from this true stress-true plastic strain relationship using Eq. (16).

5.1.2 Stage II: Cold work in corners

In the second stage, residual stresses and equivalent plastic strains defining the amount of cold work in a corner are found from a FE simulation of the large-curvature cold bending of a stainless steel sheet into a corner using ABAQUS [26], which has been introduced in Section 4 of Refs. [24,27]. the compound equivalent stress-equivalent plastic strain relationship (which reduces to the compound true stress-true plastic strain relationship in the longitudinal direction for isotropic metals) obtained from Stage I is used to define the nonlinear strain hardening behaviour of the virgin material in the FE model for cold bending.

5.1.3 Stage III: FE simulation of corner coupon tests

In the third stage, the full-range stress-strain behaviour and fracture strain of corner materials are determined by a FE simulation of the tension test of corner specimens using ABAQUS [26]. The residual stresses and equivalent plastic strains obtained from Stage II as well as an initial geometrical imperfection (to trigger diffuse necking) are introduced as the initial conditions into the FE model of the corner specimen. Again, the compound equivalent stress-equivalent plastic strain relationship obtained from Stage I is used to define the nonlinear strain-hardening behaviour of the virginal material in the FE model of the corner specimen.

5.2 Determination of the compound stress-strain relationship of virgin sheets

5.2.1 General

As mentioned in the preceding subsection, in order to determine the equivalent stress- equivalent plastic strain relationship of virgin materials for strains up to fracture, a FE simulation of the tension test of the virgin material has been carried out using ABAQUS [26]. Both geometrical and material nonlinearities were considered. Each flat tension specimen of the virgin material was modelled with the S4R shell element, which is a three-dimensional 4-node general-purpose shell element with reduced integration and hourglass control. This element is capable of handling large strains and large rotations. To trigger diffuse necking, two initial notches (i.e., geometrical imperfections) characterized by the notch radius R and width reduction ΔW were introduced to both sides of the flat specimen in the width direction at the mid-length (Fig. 7). The magnitudes of the notch radius R and width reduction ΔW were taken as $3W$ and $0.002W$ (where W is the width of the specimen and W = 12.5 mm herein) respectively. These imperfection magnitudes employed in the present study are discussed later in this section.

In modelling the flat tension coupon test, only half of the portion over the gauge length was included with symmetric conditions properly imposed in the half-portion model at the mid-length section of the flat specimen (Fig. 7). The other end (the so-called loaded end) of the half portion was subjected to a prescribed displacement. By means of kinematic coupling, the axial displacements (i.e., displacements in the length direction), the out-of-plane and in-plane rotations of all nodes at the loaded end were constrained to the rigid body motion of a reference node located at the mid-width on the loaded end. The reference node was restrained in all degrees of freedom except for the axial translation of the reference node. The testing process was achieved by specifying the desired amount of the axial displacement of the reference node, and the instantaneous axial displacement and reaction at the reference node were used to calculate the nominal stresses and nominal strains.

As shown in Eq. (16), the effect of material anisotropy on the nonlinear strain-hardening behaviour depends on the multiplication factor $3(F+G)/2(F+G+H)$. As the multiplication factor approaches to unit, the effect of material anisotropy becomes negligible. In the present study, the multiplication factors of the grade 304 sheets were 1.01 and 0.95 for the first and second batches of flat coupon tests respectively, while the factors of the grade 316L sheets were 1.10 and 1.19 for the first and second batches respectively. Therefore, the material anisotropy was taken into account in the FE model for the grade 316L sheets, but was ignored for the grade 304 sheets. The modelling of material nonlinearity for these stainless steel sheets is presented below, while the modelling of material anisotropy for the grade 316L sheets is explained in the next subsection.

To model the nonlinear strain-hardening behaviour of materials for the grade 304 sheets, a compound true stress-true plastic strain relationship in the longitudinal direction, defined by a trial weight constant w, was constructed to generate the input data for strains up to the fracture strain. For the grade 316L sheets, a compound equivalent stress-equivalent plastic strain relationship was defined as the input data through the compound true stress-true plastic strain relationship and Eq. (16). The weight constant w was varied in the FE model until the FE predicted nominal stress-strain curve agrees closely with the measured stress-strain curve. The maximum nominal strain $\varepsilon_{n,\max}$ of the flat specimen at fracture, which is defined as the percentage elongation over the gauge length, can be determined from the FE predicted elongation at which the mean value of equivalent plastic strains across the width at the mid-length section (i.e., the necking zone) is equal to $\overline{\varepsilon}_{p,f}$.

For accurate predictions, a mesh convergence study has been carried out to obtain the final mesh as shown in Fig. 7, and the flat specimen SB-304-LT was selected for the mesh study. The adopted mesh consists of 32 elements across the width and 82 elements along the length. A higher mesh density with a smaller element size was used near the mid-length section where the

initial geometrical imperfection was introduced and the diffuse necking took place. The nominal ultimate stress and the percentage elongation over a 50-mm gauge length predicted by the adopted mesh differ from reference values (values obtained from the finest mesh of 48×111 elements) by 0.01% and 1.2% respectively. These differences are taken to be satisfactory.

5.2.2 Material anisotropy

In order to define material anisotropy in ABAQUS, the local coordinate system needs to be defined for the material orientations of each shell element in the FE model. In this local coordinate system, the 1- and the 2-directions of each element are on the plane of the shell element, while the 3-direction is normal to this plane and is referred to as the normal direction. The local 1-direction coincides with the width direction of the flat specimen while the local 2-direction coincides with the length direction (or the so-called axial direction in tension tests) of the specimen. Therefore, for longitudinal flat specimens modelled in the presented study, the local 1-direction is also the transverse direction of the stainless steel sheet and the local 2-direction is also the longitudinal direction of the sheet.

In the FE model, material anisotropy is described using the orthotropic elasticity model and the anisotropic metal plasticity model available in ABAQUS. The orthotropic elasticity model is defined by the following engineering constants: elastic moduli E_1, E_2, E_3; Poisson's ratios ν_{12}, ν_{13}, ν_{23}; and shear moduli G_{12}, G_{13} and G_{23}. For these engineering constants, the subscripts 1, 2 and 3 denote the local 1-, 2- and 3-directions respectively of each shell element.

In the present FE model, the moduli E_1 and E_2 in the orthotropic elasticity model were taken as the initial elastic moduli for the transverse and longitudinal directions respectively. Since the modulus E_3 is the initial elastic modulus in the through-thickness direction, which is not available and inconsequential, the value of E_3 was taken to be the same as the initial elastic modulus E_1. The Poisson's ratios ν_{12}, ν_{13} and ν_{23} was assumed to be 0.3. The shear moduli G_{12}, G_{13} and G_{23} were taken to be 75 GPa which is the value of the initial shear elastic modulus of austenitic alloys given in Appendix B of AS/NZS 4673 [4]. It should be noted that the values of ν_{12}, ν_{13}, ν_{23}, G_{12}, G_{13} and G_{23} are inconsequential even they were given reasonable values from different sources.

The anisotropic metal plasticity model in ABAQUS is characterized by Hill's yield criterion [23] for anisotropic materials and the flow rule with isotropic hardening. The state of plastic anisotropy is defined by means of the following six yield stress ratios R_{ij}:

$$R_{11} = \frac{\sigma_{0,11}}{\sigma_0};\ R_{22} = \frac{\sigma_{0,22}}{\sigma_0};\ R_{33} = \frac{\sigma_{0,33}}{\sigma_0};\ R_{12} = \frac{\tau_{0,12}}{\tau_0};\ R_{13} = \frac{\tau_{0,13}}{\tau_0};\ R_{23} = \frac{\tau_{0,23}}{\tau_0} \qquad (20)$$

where $\sigma_{0,ii}$ is the measured initial yield stress in the i-direction, $\tau_{0,ij}$ is the measured initial shear yield stress for the i-j plane, σ_0 is the reference yield stress and $\tau_0 = \sigma_0 / \sqrt{3}$. The reference yield stress σ_0 was taken as the equivalent stress $\overline{\sigma}$ converted from the 0.2% proof stress σ_{0L} in the longitudinal direction [24,25], and is thus given by

$$\sigma_0 = \sqrt{\frac{3}{2}\left(\frac{F+G}{F+G+H}\right)}\sigma_{0L} \qquad (21)$$

where F, G and H are the anisotropy parameters defined by Eq. (10).

The initial yield stresses $\sigma_{0,ii}$ were taken to be the 0.2% proof stresses in the three principal directions, in which the through-thickness 0.2% proof stress σ_{0N} was approximated by the diagonal 0.2% proof stress σ_{0D} (i.e. $\sigma_{0N} \cong \sigma_{0D}$) [24,25]. The shear yield stress $\tau_{0,12}$ was approximated by $\sigma_{0D} / \sqrt{3}$ [28]. Both $\tau_{0,13}$ and $\tau_{0,23}$ were taken as τ_0 such that $R_{13} = 1$ and $R_{23} = 1$.

The values of all these engineering constants for the two grade 316L sheets have been obtained from flat tension coupon tests and other sources as shown above. They are summarized in Table 3.

5.2.3 Geometrical imperfections

Since the diffuse necking spreads over a length of the order of the width W, it is reasonable to assume that the magnitudes of initial geometrical imperfections, such as the notch radius R and width reduction ΔW, are proportional to the width W. A preliminary study with different values of the notch radius R and width reduction ΔW has been carried for the flat specimen SB-304-LT, and numerical results from the study are shown in Figs. 8 and 9. As shown in Fig. 8, the magnitude of the notch radius R does not affect the FE predicted nominal stress-strain curve. As shown in Fig. 9, when the notch radius is kept as a constant (i.e., $R = 3W$), the variation of the width reduction has a negligible influence on the FE prediction for $\Delta W \le 0.005W$. However, the use of $\Delta W > 0.005W$ (e.g., $\Delta W = 0.01W$, $0.02W$) will underestimate the maximum nominal strain $\varepsilon_{n,\max}$ at fracture. On the hand, according to specifications in AS 1391:1991 [18], the maximum variation of the width within the parallel length of a flat tension specimen with a 12.5-mm width should not be larger than 0.06mm. It is equivalent to a width reduction $\Delta W = 0.0024W$. Thus, a magnitude of the width reduction, which is less than $0.005W$ and follows specifications in AS 1391:1991 [18], should be selected. Therefore, an intermediate magnitude of the notch radius $R = 3W$ and a magnitude of the width reduction $\Delta W = 0.002W$ were adopted in the FE model.

5.2.4 Predictions of weight constants and fracture strains

Using the FE simulation of flat tension coupon tests as presented earlier, the weight constants and fracture strains of longitudinal flat specimens cut from the four stainless steel sheets were determined. Fig. 10 shows the compound true stress-true plastic strain curves (i.e., input data) of flat specimen SB-304-LT for different trial values of the weight constant w. Fig. 11 shows the comparison between the measured stress-strain curve of the flat specimen and the FE predicted nominal stress-strain curves resulting from different trial weight constants. Successful trial weight constants of longitudinal flat specimens cut from these four virgin sheets as well as the corresponding true plastic strains $\varepsilon_{tp,f}$ at fracture are shown in Table 4. It can be seen that the true plastic strains $\varepsilon_{tp,f}$ at fracture can exceed 1.0. Similar observations were also made elsewhere [15,29] for carbon steels and other sheet metals. Comparisons between measured percentage elongations after fracture and the corresponding FE predicted $\varepsilon_{n,\max}$ values for these four flat specimens are also presented in Table 4. FE predicted $\varepsilon_{n,\max}$ values are in close agreement with test results, demonstrating the accuracy of the modified weighted-average method and the predicted post-ultimate stress-strain behaviour. Representative comparisons between measured stress-strain curves and FE predicted nominal stress-strain curves of virgin sheets are shown in Fig. 12.

5.3 Nonlinear FE simulation of corner coupon tests

In order to predict the enhanced strength, the reduced ductility and even the full-range stress-strain behaviour of corner materials up to fracture, a FE simulation of the tension test of the corner material has been carried out using ABAQUS [26]. Again, both geometrical and material nonlinearities were considered. Similar to the flat specimen, each corner specimen was also modelled with the S4R shell element. Simpson's rule was used for the section integration, and 17 integration points were specified across the thickness of the shell element to allocate the residual stresses and equivalent plastic strains in the corner due to cold bending. These residual stresses and equivalent plastic strains throughout the thickness of a corner were pre-determined from a FE simulation of the large-curvature cold bending of a stainless steel sheet into a corner (i.e., the second stage of the advanced numerical approach), which has been introduced elsewhere [24,27]. These predictions of residual stresses and equivalent plastic strains were imposed into the FE model of the corner tension specimen as the initial state using the *INITIAL CONDITIONS option. Predictions of residual stresses and equivalent plastic strains in corner specimen SB-304-SCr4t2 are shown in Fig. 13. Predictions for other corner specimens are given in Ref. [30].

To trigger diffuse necking in the FE model, two initial notches were introduced to both sides of the corner specimen in the width direction at the mid-length (Fig. 14). The magnitudes of the notch radius R and width reduction ΔW were the same as those specified in the FE model of the flat specimen: $R = 3W$ and $\Delta W = 0.002W$, except that W was taken as the curved width of the corner specimen.

The mechanical properties of virgin sheets were specified in the material modelling. Using the modified weight-average method (i.e., the first stage of the advanced numerical approach), the weight constant and the corresponding compound equivalent stress-equivalent plastic strain curve of virgin sheets were resulted and employed herein to model the nonlinear strain-hardening behaviour of materials. Again, the material anisotropy was taken into account in the FE model of the corner specimen for grade 316L but was ignored for grade 304. In the modelling of material anisotropy, the local coordinate system

defined for material orientations in the FE model of the corner specimen was the same as the system used for the flat specimen. Thus, engineering constants used in the material model for the corner specimen were also the same as those for the flat specimen.

In modelling the corner tension coupon test, only half of the portion over the gauge length was included with symmetric conditions properly imposed in the half-portion model at the mid-length section of the corner specimen (Fig. 14). The other end (i.e., the loaded end) of the half portion was subjected to a prescribed displacement. By means of kinematic coupling, the axial displacements, the out-of-plane and in-plane rotations of all nodes at the loaded end were constrained to the rigid body motion of a reference node located at the centroid of the cross section on the loaded end. The reference node was restrained in all degrees of freedom except for the axial translation of the reference node. The testing process was achieved by specifying the desired amount of the axial displacement of the reference node, and the instantaneous axial displacement and reaction at the reference node were used to calculate the nominal stresses and nominal strains. Some steps were included to simulate the transverse spring-back, longitudinal natural bending and straightening of the corner specimen before the axial displacement was applied. The maximum nominal strain of the corner specimen at fracture (i.e., the percentage elongation over the gauge length) can be determined from the FE predicted elongation at which the mean value of equivalent plastic strains across the width and thickness at the mid-length section (i.e., the necking zone) is equal to $\bar{\varepsilon}_{p,f}$. The typical deformed shape of a corner specimen at the end of diffuse necking, obtained from the FE simulation, is shown in Fig. 15; and it is in close agreement with the deformed shape observed from tests.

A mesh convergence study has also been carried out to obtain the final mesh as shown in Fig. 14. The adopted mesh consists of 32 elements across the width and 82 elements along the length. Again, a higher mesh density with a smaller element size was used near the mid-length section where the initial geometrical imperfection was introduced. The nominal ultimate stress and the percentage elongation over a 50-mm gauge length predicted by the adopted mesh differ from reference values (values obtained from the finest mesh of 48×111 elements) by 0.01% and 0.9% respectively. These differences are taken to be satisfactory.

6. RESULTS AND COMPARISONS

6.1 Comparison with test results

Using the advanced numerical approach introduced in the preceding section, $\sigma_{0.2,c}$, $\sigma_{u,c}$, $\varepsilon_{50,c}$ and full-range nominal stress-strain curves have been predicted numerically for corner materials tested in the experimental program (see Section 3). These FE predictions are compared with test results and summarized in Table 5. It is seen that the proposed numerical approach can provide accurate predictions of the enhanced strength and reduced ductility of corners, with the mean values of the FE prediction to test result ratios being 1.11, 0.97 and 1.05 for $\sigma_{0.2,c}$, $\sigma_{u,c}$ and $\varepsilon_{50,c}$ respectively.

Figs. 16 and 17 show representative comparisons of full-range nominal stress-strain curves of corner specimens between FE predictions and test results for the first and second batches of tests respectively. The whole set of comparisons can be found in Ref. [30]. In Figs. 16 and 17, stress-strain curves measured by the single corner coupon test (SC) and twin corner coupon test (TC) are also compared. It is seen that stress-strain curves measured by single corner coupon tests are in close agreement with those obtained from twin corner coupon tests, which demonstrates the validity of both testing methods. From Figs. 16 and 17, it can be seen that the stress-strain curves predicted by the advanced numerical approach (F.E.A.) are generally in close agreement with experimental stress-strain curves up to the fracture strain, which further demonstrates the accuracy of the proposed approach.

6.2 Comparison with existing empirical models

Corner strengths (including $\sigma_{0.2,c}$ and $\sigma_{u,c}$) predicted by the advanced numerical approach are also compared with those obtained from existing empirical models [3,6] in this subsection. The empirical model for the prediction of $\sigma_{0.2,c}$ given in the Australian/New Zealand Standard AS/NZS 4673 [4] is only applicable to ferritic alloys, and thus it has not been included in the comparison. The empirical model proposed by Van den Berg and Van der Merwe's model [3] is only capable of predicting $\sigma_{0.2,c}$. Two empirical models, namely the simple power model and the power model, for predicting $\sigma_{0.2,c}$ were proposed by Ashraf et al. [6]. In these empirical models [3,6], $\sigma_{0.2,c}$ is expressed in terms of the r_i/t ratio, the nominal 0.2% proof stress $\sigma_{0.2,v}$ and ultimate strength $\sigma_{u,v}$ of virgin materials. A linear equation for predicting $\sigma_{u,c}$ was further proposed by Ashraf et al. [6], in which $\sigma_{u,c}$ is independent of the r_i/t ratio and is expressed in terms of $\sigma_{0.2,c}$, $\sigma_{0.2,v}$ and $\sigma_{u,v}$ as given by Eq. (22):

$$\sigma_{u,c} = 0.75\sigma_{0.2,c}\left(\frac{\sigma_{u,v}}{\sigma_{0.2,v}}\right). \quad (22)$$

Table 6 summarizes comparisons of corner 0.2% proof stresses $\sigma_{0.2,c}$ between the advanced numerical approach and three existing empirical models [3,6]. In the table, the ratio between the prediction from each method and the test result of each specimen is given for comparisons. It can be seen that Van den Berg and Van der Merwe's model [3], the simple power model and the power model [6] underestimate $\sigma_{0.2,c}$ on the average by about 40%, 10% and 20% respectively. The simple model provides better predictions than Van den Berg and Van der Merwe's model and the power model. The advanced numerical approach slightly overestimates $\sigma_{0.2,c}$ on the average by 11%. Both the advanced numerical approach and the simple power model can provide quite satisfactory predictions of $\sigma_{0.2,c}$ with similar accuracy.

Table 7 shows comparisons of corner ultimate strengths $\sigma_{u,c}$ between the advanced numerical approach and the empirical models from Ashraf et al. [6]. As shown in Table 7, two empirical predictions of $\sigma_{u,c}$ have been obtained for each specimen. One of them has been calculated using Eq. (22) with the $\sigma_{0.2,c}$ value predicted by the simple power model, while another one has been calculated based on the $\sigma_{0.2,c}$ value predicted by the power model. As seen from Table 7, both the advanced numerical approach and the linear equation (Eq. (22)) incorporating the simple power model can provide accurate predictions of $\sigma_{u,c}$ with similar accuracy. Both methods provide better predictions than the linear equation incorporating the power model. In general, the advanced numerical approach can give accurate predictions with less scatter than empirical models.

7. CONCLUSIONS

The cold forming of stainless steel sections induces cold work in the member, which can enhance the strength but reduce the ductility of the material. In the nonlinear FE analysis of the structural behaviour of cold-formed stainless steel members, the stress-strain relationship of the material in corners (i.e., corner materials) would be required to produce accurate numerical predictions. This paper has been concerned with the accurate prediction of the enhanced strength, reduced ductility and stress-strain behaviour of the corner material in cold-formed stainless steel sections by presenting an advanced numerical approach for the simulation of corner coupon tests. This advanced numerical approach can overcome the limitations of the existing theoretical and empirical models, and has been implemented using the FE package ABAQUS [26] to demonstrate its accuracy and capability.

The cold work in the corner of a cold-formed section is quantified using the co-existent residual stresses and equivalent plastic strains with the latter representing the level of strain hardening of the material. The enhanced strength and reduced ductility of corner materials are attributed to these residual stresses and equivalent plastic strains in the corner as well as the strain-hardening capability arising from the post-ultimate true stress-true plastic strain behaviour of virgin sheets (see Fig. 10). Thus, cold forming allows this post-ultimate strain-hardening capability of virgin sheets to be utilized in cold-worked materials, and explains why the ultimate strength of corner materials can be increased to exceed the ultimate strength of virgin sheets. The proposed numerical approach has taken account of the aforementioned characteristics of sheet metals after cold working.

In the present paper, a modified weighted-average method has been first presented to predict the post-ultimate stress-strain behaviour of virgin stainless steel sheets up to the fracture strain. By incorporating this modified weighted-average method, the advanced numerical approach has been next presented for predicting the enhanced stress-strain behaviour and reduced ductility of corner materials in cold-formed stainless steel sections. In this approach, the effect of cold work in the corner has been taken into account by means of a FE simulation of the cold forming of corners, with the resulting residual stresses and equivalent plastic strains specified as the initial state in a subsequent FE simulation of corner coupon tests. Tests of corner materials cut from press-braked stainless steel sections have been performed and test results have also been presented in the paper. Numerical predictions from the proposed approach have been shown to agree closely with test results, demonstrating the accuracy of the approach.

It should be noted that lower bound solutions of the corner ductility and formability of cold-formed stainless steel sections can be found using the power-law extrapolation (i.e., the weight constant w = 0) (see Eqs. (4) and (18)) for the post-ultimate stress-strain behaviour of virgin sheets in the advanced numerical approach. These lower bound solutions can be deployed in

future research to advance ductility requirements to avoid corner cracking and permit adequate structural performance. It is also important to note that the modified weighted-average method and the general principles of the advanced numerical approach are applicable to various cold-worked materials produced from all types of sheet metals and different cold-forming processes for the assessment of their altered mechanical behaviour and its effect on the structural performance.

ACKNOWLEDGEMENTS
The authors are grateful for the financial support provided by The University of Macau (Ref. No. RG061/09-10S/12R/QWM/FST), and the Fundo para o Desenvolvimento das Ciências e da Tecnologia (FDCT) of the Macao S.A.R. (Ref. No. 011/2007/A1).

REFERENCES

[1] K.W. Karren, Material properties models for analysis of cold-formed steel members, *Journal of the Structural Division, ASCE*. 93(ST1) (1967) 401-432.
[2] J.S. Coetsee, G.J. Van den Berg, P. Van der Merwe, The effect of work hardening and residual stresses due to cold work of forming on the strength of cold-formed stainless steel lipped channel sections. *Proceedings of the Tenth International Specialty Conference on Cold-Formed Steel Structures*, St.Louis, Missouri, United States, 23-24 October, 1990, pp. 505-523.
[3] G.J. Van den Berg, P. Van der Merwe, Prediction of corner mechanical properties fro stainless steels due to clod forming, *Proceedings of the Eleventh International Specialty Conference on Cold-Formed Steel Structures*, St. Louis, Missouri, United States, 20-21 October, 1992, pp. 571-586.
[4] AS/NZS, *Cold-Formed Stainless Steel Structures. AS/NZS 4673:2001*, Australian/New Zealand Standard, Sydney, Australia, 2001.
[5] L. Gardner, D.A. Nethercot, Experiments on stainless steel hollow sections – Part 1: Material and cross-sectional behaviour, *Journal of Constructional Steel Research.* 60 (2004) 1291-1318.
[6] M. Ashraf, L. Gardner, D. A. Nethercot, Strength enhancement of the corner regions of stainless steel cross-sections, *Journal of Constructional Steel Research.* 61 (2005) 37-52.
[7] R.B. Cruise, L. Gardner, Strength enhancements induced during cold forming of stainless steel sections, *Journal of Constructional Steel Research.* 64 (2008) 1310-1316.
[8] R. Greiner, M. Kettler, Interaction of bending and axial compression of stainless steel members, *Journal of Constructional Steel Research.* 64 (2008) 1217-1224.
[9] B. Ross, H. Degée, F. Pascon, Enhanced mechanical properties after cold process of fabrication of non-linear metallic profiles, *Thin-Walled Structures.* 47 (2009) 1575-1589.
[10] F.A. McClintock, Z.M. Zheng, Ductile fracture in sheets under transverse strain gradients, *Journal of Fracture.* 64 (1993) 321-337.
[11] Y. Ling, Uniaxial true stress-strain after necking, *AMP Journal of Technology.* 5 (1996) 37-48.
[12] Z.L. Zhang, M. Hauge, J. Ødegård, C. Thaulow, Determining material true stress-strain curve from tensile specimens with rectangular cross-section, *International Journal of Solids and Structures.* 36 (1999) 3497-3516.
[13] P. Koc, B. Štok, Computer-aided identification of the yield curve of a sheet metal after onset of necking, *Computational Materials Science.* 31 (2004) 155-168.
[14] Y.B. Bao, Dependence of ductile crack formation in tensile tests on stress triaxiality, stress and strain ratios, *Engineering Fracture Mechanics.* 72 (2005) 505-522.
[15] M.S. Joun, J.G. Eom, M.C. Lee, A new method for acquiring true stress–strain curves over a large range of strains using a tensile test and finite element method, *Mechanics of Materials.* 40 (2008) 586-593.
[16] K.J.R. Rasmussen, Full-range stress-strain curves for stainless steel alloys, *Journal of Constructional Steel Research.* 59 (2003) 47-61.
[17] W.M. Quach, J.G. Teng, K.F. Chung, Three-stage full-range stress-strain model for stainless steels, *Journal of Structural Engineering, ASCE.* 134(9) (2008) 1518-1527.
[18] AS, *Methods for Tensile Testing of Metals. AS 1391:1991*, Australian/New Zealand Standard, Sydney, Australia, 1991.
[19] A. Considère, L'emploi du fer de l'acier dans les constructions, *Annales des Ponts er Chaussées IX9.* 6 eme serie (1885) 574-595.
[20] J. Chakrabarty, *Applied Plasticity*, Springer-Verlag Inc., New York, 2000.
[21] R. Hill, On discontinuous plastic states, with special reference to localized necking in thin sheets, *Journal of the Mechanics and Physics of Solids.* 1 (1952) 19-30.
[22] A.R. Ragab, S.E. Bayoumi, *Engineering Solid Mechanics: Fundamentals and Applications*, CRC press, United States, 1998.
[23] R. Hill, *The Mathematical Theory of Plasticity*, Oxford University Press, United States, 1950.
[24] W.M. Quach, J.G. Teng, K.F. Chung, Residual stresses in press-braked stainless steel sections – I: Coiling and uncoiling of sheets, *Journal of Constructional Steel Research.* 65 (2009) 1803-1815.
[25] W.M. Quach, J.G. Teng, K.F. Chung, Effect of the manufacturing process on the behaviour of press-braked thin-walled steel columns, *Engineering Structures.* 32 (2010) 3501-3515.
[26] ABAQUS, *Standard User's Manual, Version 6.5*, Hibbit, Karlsson and Sorensen, Inc., United States, 2004.
[27] W.M. Quach, J.G. Teng, K.F. Chung, Residual stresses in press-braked stainless steel sections – II: Press-braking operations, *Journal of Constructional Steel Research.* 65 (2009) 1816-1826.
[28] K.J.R. Rasmussen, T. Burns, P. Bezkorovainy, M.R. Bambach, Numerical modelling of stainless steel plates in compression, *Journal of Constructional Steel Research.* 59 (2003) 1345-1362.
[29] K.H. Nip, L. Gardner, C.M. Davies, A.Y. Elghazouli, Extremely low cycle fatigue tests on structural carbon steel and stainless steel, *Journal of Constructional Steel Research.* 66 (2010) 96-110.
[30] P. Qiu, *Stress-Strain Behaviour of Cold-Worked Materials in Cold-Formed Stainless Steel Sections, MSc Thesis*, Department of Civil and Environmental Engineering, University of Macau, Macau S.A.R., China, 2011.

Table 1. Measured mechanical properties of virgin sheets for the longitudinal direction.

Sheet*	E_0 (GPa)	n	$\sigma_{0.2,v}$ (MPa)	$\sigma_{u,v}$ (MPa)	$\varepsilon_{u,v}$
FB-304-LT	200.6	5.36	277.1	784.1	0.64
FB-316L-LT	180.4	5.34	260.7	596.5	0.57
SB-304-LT	200.1	4.42	240.2	699.7	0.75
SB-316L-LT	187.4	3.10	234.1	564.5	0.53
* LT = Longitudinal tension.					

Table 2. Measured geometrical and mechanical properties of corner specimens.

Specimen	r_i/t	$\sigma_{0.2,c}$ (MPa)	$\sigma_{u,c}$ (MPa)	$\varepsilon_{50,c}$	$\frac{\sigma_{0.2,c}}{\sigma_{0.2,v}}$	$\frac{\sigma_{u,c}}{\sigma_{u,v}}$
FB-304-SCr4t2	2.0	463.4	854.2	N.A.*	1.67	1.09
FB-304-TCr4t2	2.0	483.6	891.6	0.503	1.75	1.14
FB-304-SCr6t2	3.0	374.9	815.3	0.545	1.35	1.04
FB-304-TCr6t2	3.0	373.8	844.2	0.553	1.35	1.08
SB-304-SCr4t2-1	2.0	428.2	812.2	0.685	1.78	1.16
SB-304-SCr4t2-2	2.0	437.3	816.8	0.675	1.82	1.17
SB-304-SCr4t2-3	2.0	473.2	829.7	0.646	1.97	1.19
SB-304-SCr6t2-1	3.0	419.0	827.6	0.715	1.74	1.18
SB-304-SCr6t2-2	3.0	407.7	787.4	0.648	1.70	1.13
SB-304-SCr6t2-3	3.0	414.8	814.5	0.668	1.73	1.16
SB-304-TCr6t2-1	3.0	394.4	784.4	0.661	1.64	1.12
SB-304-TCr6t2-2	3.0	405.6	791.3	0.681	1.69	1.13
FB-316L-SCr4t2	2.1	415.3	626.5	N.A.	1.59	1.05
FB-316L-TCr4t2	2.1	441.0	687.4	0.509	1.69	1.15
FB-316L-SCr6t2	3.0	434.1	645.6	N.A.	1.67	1.08
FB-316L-TCr6t2	3.1	409.3	666.1	0.562	1.57	1.12
SB-316L-SCr4t2-1	2.0	459.9	681.5	0.424	1.96	1.21
SB-316L-SCr4t2-2	2.0	428.9	651.7	0.402	1.83	1.15
SB-316L-SCr4t2-3	2.0	462.0	681.5	0.437	1.97	1.21
SB-316L-SCr6t2-1	3.0	431.0	660.9	0.468	1.84	1.17
SB-316L-SCr6t2-2	3.0	429.6	658.6	0.478	1.84	1.17
SB-316L-SCr6t2-3	3.0	428.2	660.2	0.474	1.83	1.17
SB-316L-TCr6t2-1	3.0	420.3	672.3	0.482	1.80	1.19
SB-316L-TCr6t2-2	3.0	397.1	645.1	0.561	1.70	1.14
Mean					1.73	1.14
Standard deviation					0.16	0.05
* N.A. = the measured value is not available as fracture occurred outside the gauge length.						

Table 3. Engineering constants for the two grade 316L stainless steel sheets.

Sheet	E_1 (GPa)	E_2 (GPa)	E_3 (GPa)	σ_0 (MPa)	τ_0 (MPa)	$\sigma_{0,11}$ (MPa)	$\sigma_{0,22}$ (MPa)	$\sigma_{0,33}$ (MPa)	$\tau_{0,12}$ (MPa)	$\tau_{0,13}$ (MPa)	$\tau_{0,23}$ (MPa)
FB-316L	205	180	205	273.0	157.6	287.1	260.7	272.9	157.6	157.6	157.6
SB-316L	215	187	215	255.9	147.7	274.8	234.1	264.1	152.5	147.7	147.7

Table 4. Weight constants w and fracture strains of flat specimens.

Specimen*	Weight constant w	True plastic strain $\varepsilon_{tp,f}$ at fracture	Percentage elongation $\varepsilon_{n,\max}$		
			Test result (1)	FE prediction (2)	$\frac{(2)}{(1)}$
FB-304-LT	0.0	0.98	0.728	0.768	1.05
FB-316L-LT	0.375	0.95	0.793	0.757	1.05
SB-304-LT	0.5	1.31	0.848	0.865	0.98
SB-316L-LT	1.0	1.31	0.691	0.683	0.99
* LT = Longitudinal flat tension specimen.					

Table 5. FE predictions of corner mechanical properties.

Specimen	$\sigma_{0.2,c}$		$\sigma_{u,c}$		$\varepsilon_{50,c}$	
	FE prediction (MPa)	$\frac{FE}{Test}$ *	FE prediction (MPa)	$\frac{FE}{Test}$	FE prediction	$\frac{FE}{Test}$
FB-304-SCr4t2	534.4	1.15	874.4	1.02	0.507	N.A.#
FB-304-TCr4t2	534.4	1.11	874.4	0.98	0.507	1.01
FB-304-SCr6t2	474.1	1.26	848.8	1.04	0.558	1.02
FB-304-TCr6t2	474.1	1.27	848.8	1.01	0.558	1.01
SB-304-SCr4t2-1	502.7	1.17	779.2	0.96	0.662	0.97
SB-304-SCr4t2-2	502.7	1.15	779.2	0.95	0.662	0.98
SB-304-SCr4t2-3	502.7	1.06	779.2	0.94	0.662	1.02
SB-304-SCr6t2-1	443.9	1.06	755.9	0.91	0.739	1.03
SB-304-SCr6t2-2	443.9	1.09	755.9	0.96	0.739	1.14
SB-304-SCr6t2-3	443.9	1.07	755.9	0.93	0.739	1.11
SB-304-TCr6t2-1	443.9	1.13	755.9	0.96	0.739	1.12
SB-304-TCr6t2-2	443.9	1.09	755.9	0.96	0.739	1.09
FB-316L-SCr4t2	507.7	1.22	670.6	1.07	0.465	N.A.
FB-316L-TCr4t2	507.7	1.15	670.6	0.98	0.465	0.91
FB-316L-SCr6t2	450.2	1.04	648.3	1.00	0.530	N.A.
FB-316L-TCr6t2	450.2	1.10	648.3	0.97	0.530	0.94
SB-316L-SCr4t2-1	493.9	1.07	643.5	0.94	0.460	1.08
SB-316L-SCr4t2-2	493.9	1.15	643.5	0.99	0.460	1.14
SB-316L-SCr4t2-3	493.9	1.07	643.5	0.94	0.460	1.05
SB-316L-SCr6t2-1	442.1	1.03	620.2	0.94	0.537	1.15
SB-316L-SCr6t2-2	442.1	1.03	620.2	0.94	0.537	1.12
SB-316L-SCr6t2-3	442.1	1.03	620.2	0.94	0.537	1.13
SB-316L-TCr6t2-1	442.1	1.05	620.2	0.92	0.537	1.11
SB-316L-TCr6t2-2	442.1	1.11	620.2	0.96	0.537	0.96
Mean		1.11		0.97		1.05
Standard deviation		0.07		0.04		0.07
* FE = Finite element prediction; Test = Test result. # N.A. = the measured value is not available as fracture occurred outside the gauge length.						

Table 6. Comparisons of FE predictions of corner 0.2% proof stresses with predictions from existing empirical models.

Specimen	$(\sigma_{0.2,c})_{pred} / (\sigma_{0.2,c})_{test}$ *			
	Van den Berg and Van der Merwe (1992)	Ashraf et al. (2005) – Simple power model	Ashraf et al. (2005) – Power model	F.E.A.
FB-304-SCr4t2	0.56	0.98	0.84	1.15
FB-304-TCr4t2	0.53	0.94	0.80	1.11
FB-304-SCr6t2	0.64	1.12	0.90	1.26
FB-304-TCr6t2	0.64	1.13	0.90	1.27
SB-304-SCr4t2-1	0.45	0.92	0.76	1.17
SB-304-SCr4t2-2	0.44	0.90	0.74	1.15
SB-304-SCr4t2-3	0.41	0.83	0.69	1.06
SB-304-SCr6t2-1	0.43	0.87	0.67	1.06
SB-304-SCr6t2-2	0.44	0.90	0.69	1.09
SB-304-SCr6t2-3	0.43	0.88	0.68	1.07
SB-304-TCr6t2-1	0.45	0.93	0.71	1.13
SB-304-TCr6t2-2	0.44	0.90	0.69	1.09
FB-316L-SCr4t2	0.93	1.03	1.00	1.22
FB-316L-TCr4t2	0.88	0.97	0.94	1.15
FB-316L-SCr6t2	0.84	0.91	0.87	1.04
FB-316L-TCr6t2	0.89	0.96	0.92	1.10
SB-316L-SCr4t2-1	0.71	0.83	0.80	1.07
SB-316L-SCr4t2-2	0.76	0.89	0.86	1.15
SB-316L-SCr4t2-3	0.71	0.83	0.79	1.07
SB-316L-SCr6t2-1	0.71	0.82	0.76	1.03
SB-316L-SCr6t2-2	0.71	0.83	0.77	1.03
SB-316L-SCr6t2-3	0.71	0.83	0.77	1.03
SB-316L-TCr6t2-1	0.73	0.84	0.78	1.05
SB-316L-TCr6t2-2	0.77	0.89	0.83	1.11
Mean	0.63	0.91	0.80	1.11
Standard deviation	0.17	0.08	0.09	0.07
* Subscripts: *pred* = Prediction; *test* = Test result.				

Table 7. Comparisons of FE predictions of corner ultimate strengths with predictions from existing empirical models.

Specimen	$(\sigma_{u,c})_{pred} / (\sigma_{u,c})_{test}$ *		
	Ashraf et al. (2005) – Simple power model	Ashraf et al. (2005) – Power model	F.E.A.
FB-304-SCr4t2	1.13	0.96	1.02
FB-304-TCr4t2	1.08	0.92	0.98
FB-304-SCr6t2	1.10	0.88	1.04
FB-304-TCr6t2	1.06	0.85	1.01
SB-304-SCr4t2-1	1.06	0.87	0.96
SB-304-SCr4t2-2	1.06	0.87	0.95
SB-304-SCr4t2-3	1.04	0.86	0.94
SB-304-SCr6t2-1	0.96	0.74	0.91
SB-304-SCr6t2-2	1.01	0.78	0.96
SB-304-SCr6t2-3	0.98	0.75	0.93
SB-304-TCr6t2-1	1.02	0.78	0.96
SB-304-TCr6t2-2	1.01	0.78	0.96
FB-316L-SCr4t2	1.17	1.14	1.07
FB-316L-TCr4t2	1.06	1.04	0.98
FB-316L-SCr6t2	1.05	1.00	1.00
FB-316L-TCr6t2	1.02	0.97	0.97
SB-316L-SCr4t2-1	1.02	0.97	0.94
SB-316L-SCr4t2-2	1.07	1.02	0.99
SB-316L-SCr4t2-3	1.02	0.97	0.94
SB-316L-SCr6t2-1	0.97	0.90	0.94
SB-316L-SCr6t2-2	0.98	0.90	0.94
SB-316L-SCr6t2-3	0.97	0.90	0.94
SB-316L-TCr6t2-1	0.96	0.88	0.92
SB-316L-TCr6t2-2	1.00	0.92	0.96
Mean	1.03	0.90	0.97
Standard deviation	0.05	0.10	0.04

* Subscripts: *pred* = Prediction; *test* = Test result.

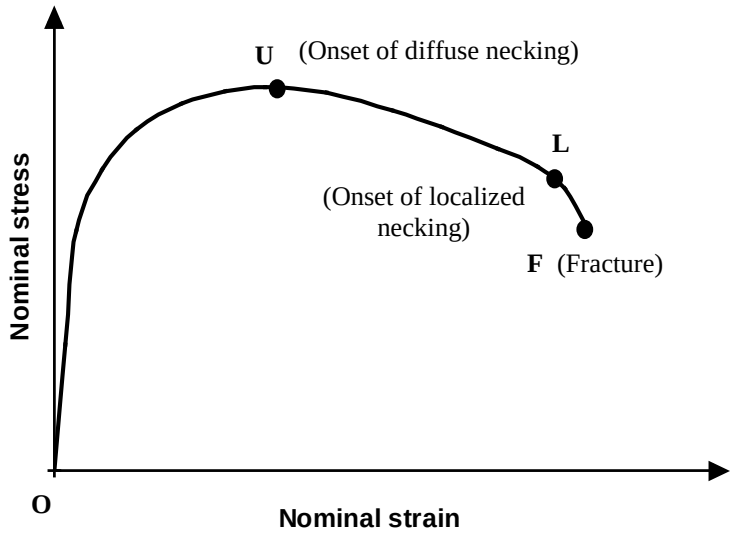

Fig. 1. Schematic plot of a typical nominal stress-strain curve for a flat tension specimen (reproduced from Ref. [12]).

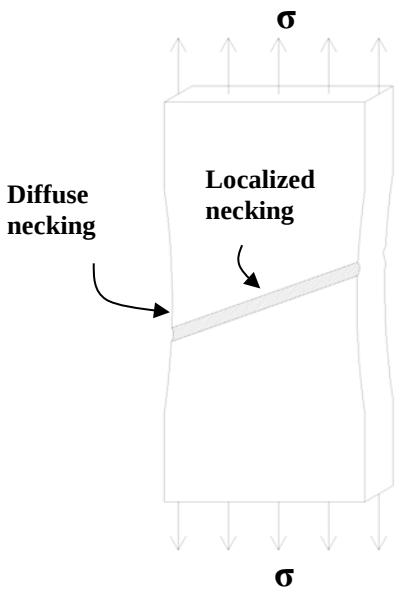

Fig. 2. Necking of a flat metal strip.

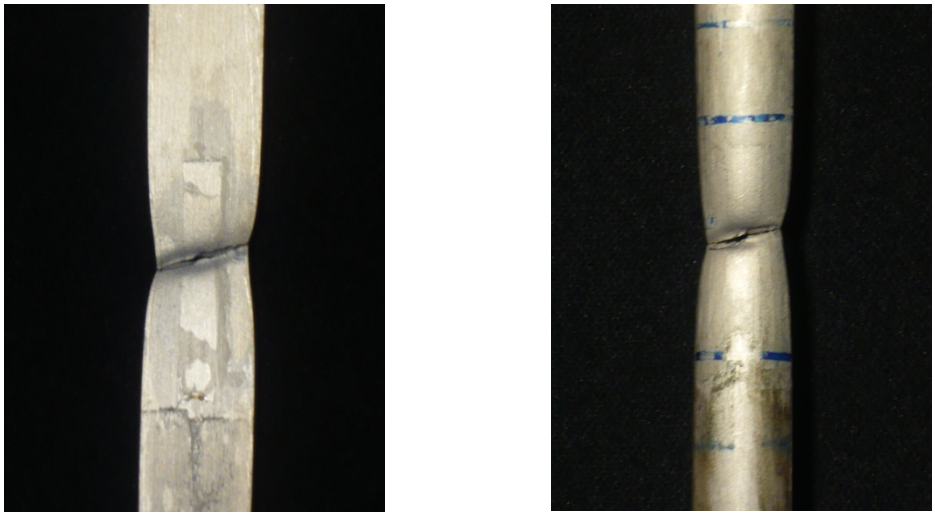

(a) Flat specimen (b) Corner specimen

Fig. 3. Typical deformed shapes of tension specimens after fracture.

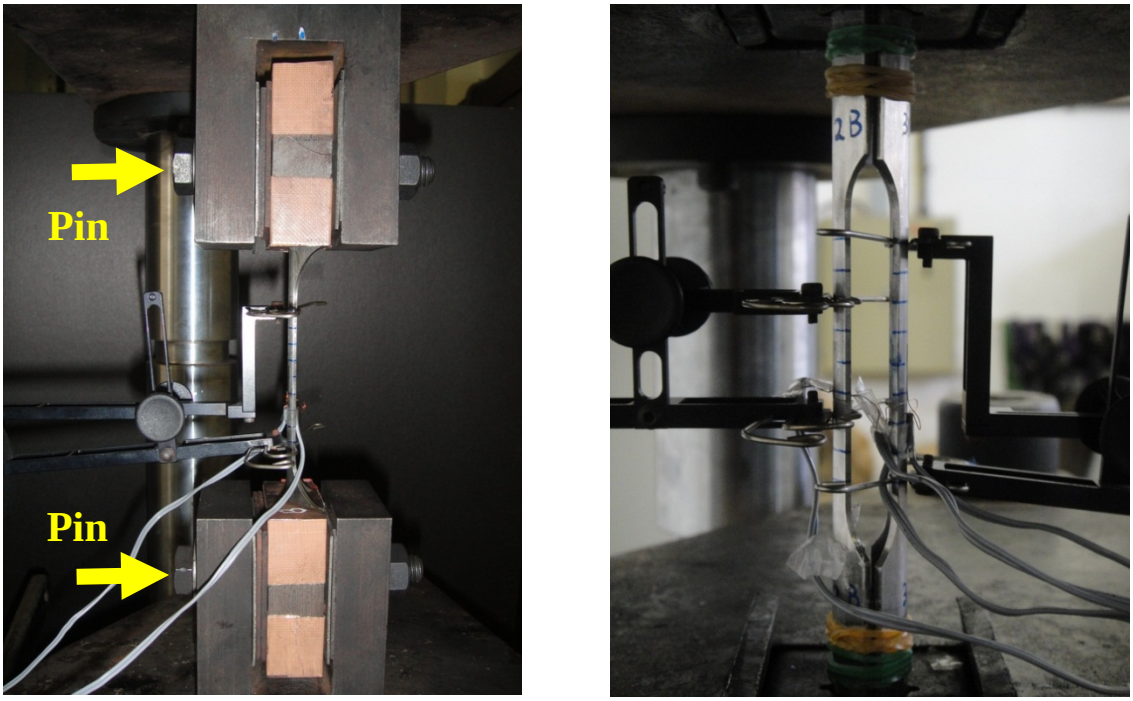

(a) Single corner coupon test (SC)

(b) Twin corner coupon test (TC)

Fig. 4. Test setup.

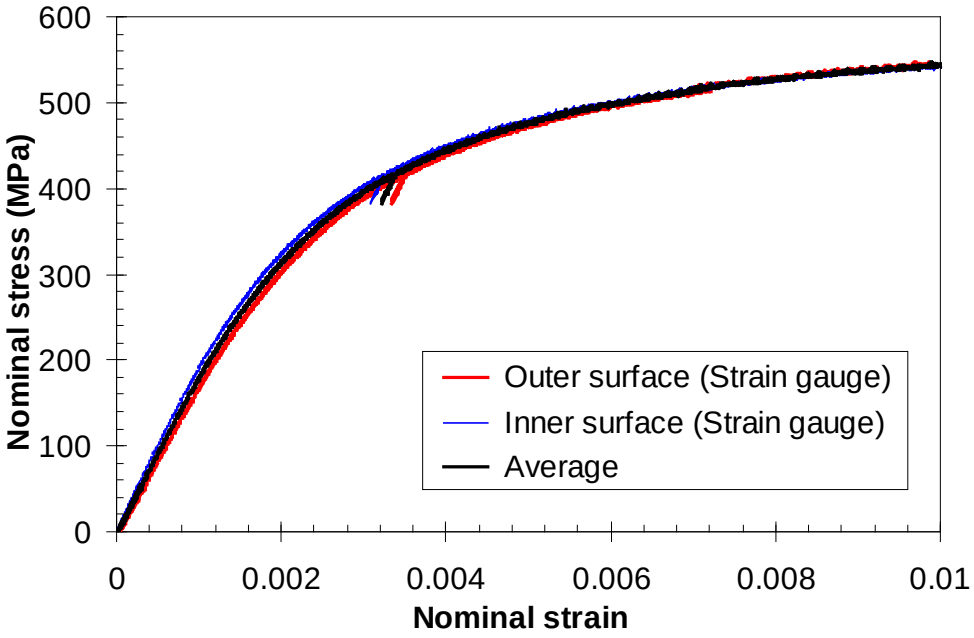

(a) Specimen FB-304-SCr4t2

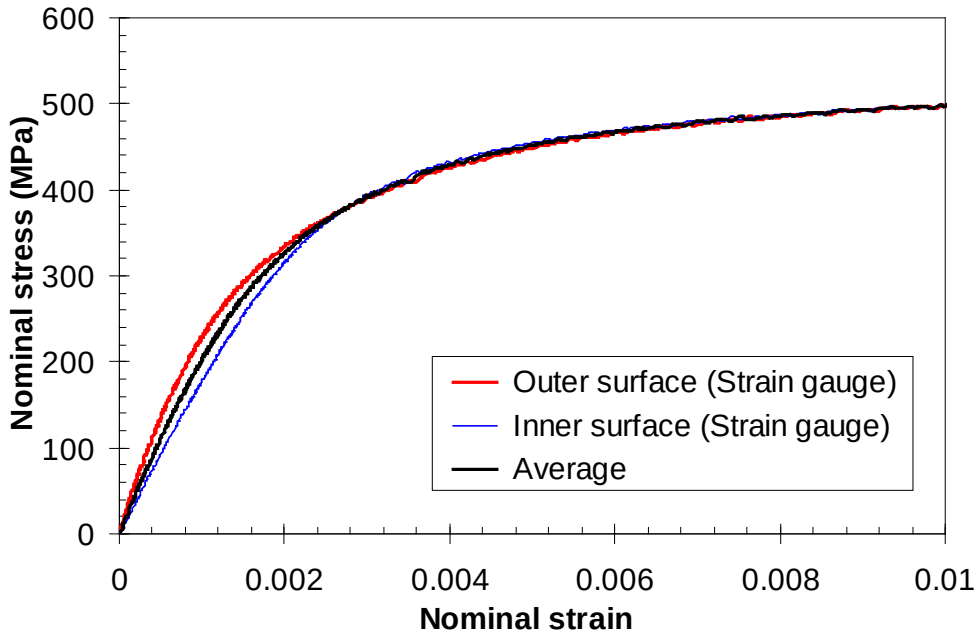

(b) Specimen SB-304-SCr4t2-1

Fig. 5. Initial stress-strain curves of single corner specimens measured by strain gauges.

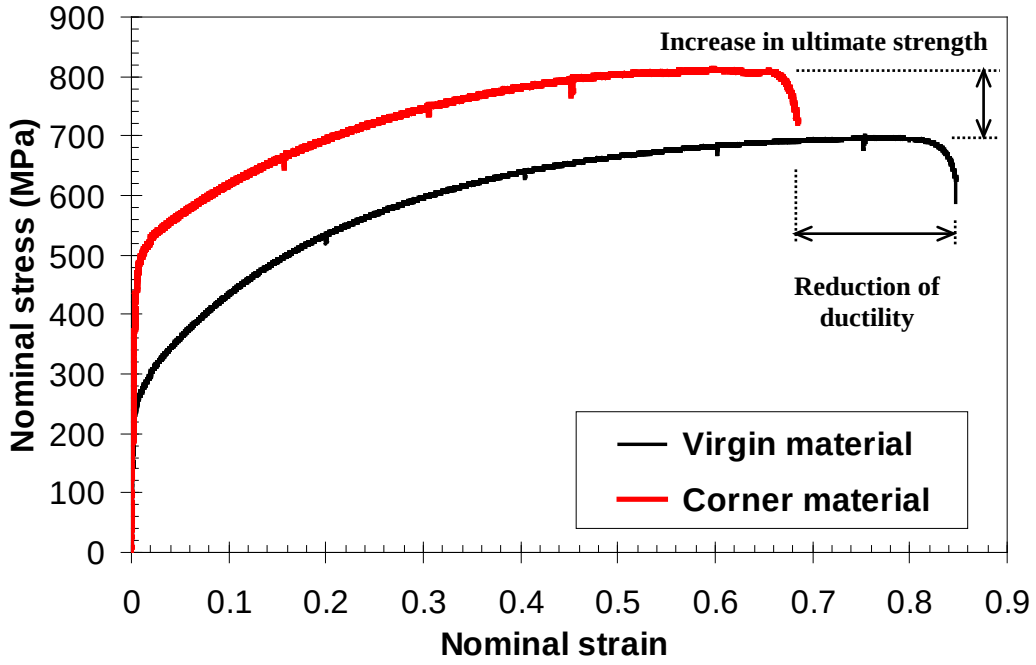

(a) Full stress-strain curves

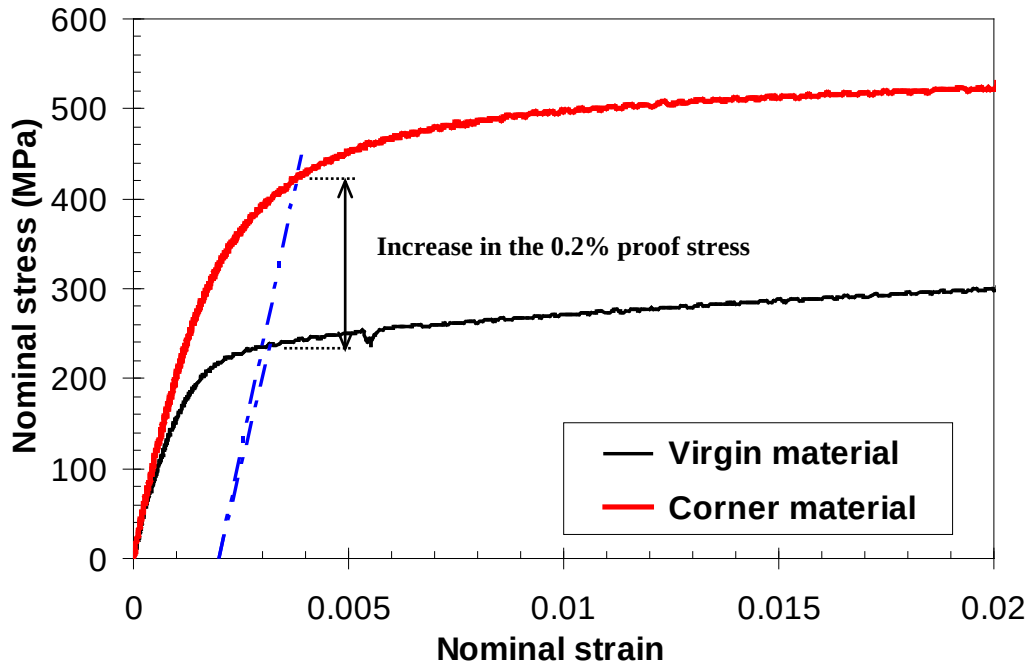

(b) Initial stress-strain curves

Fig. 6. Effect of cold work on the stress-strain behaviour of the corner material (specimen SB-304-SCr4t2-1) from a press-braked stainless steel section.

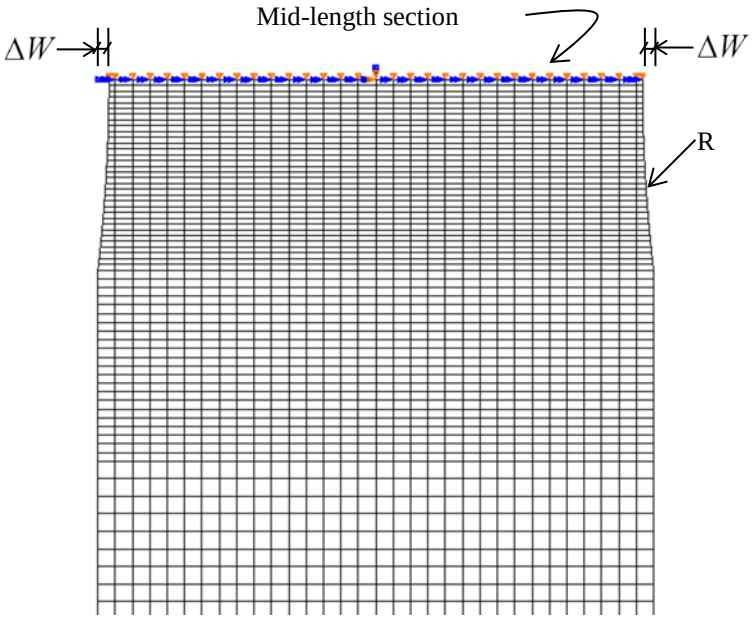

Fig. 7. Initial notches imposed in the FE model of a flat specimen.

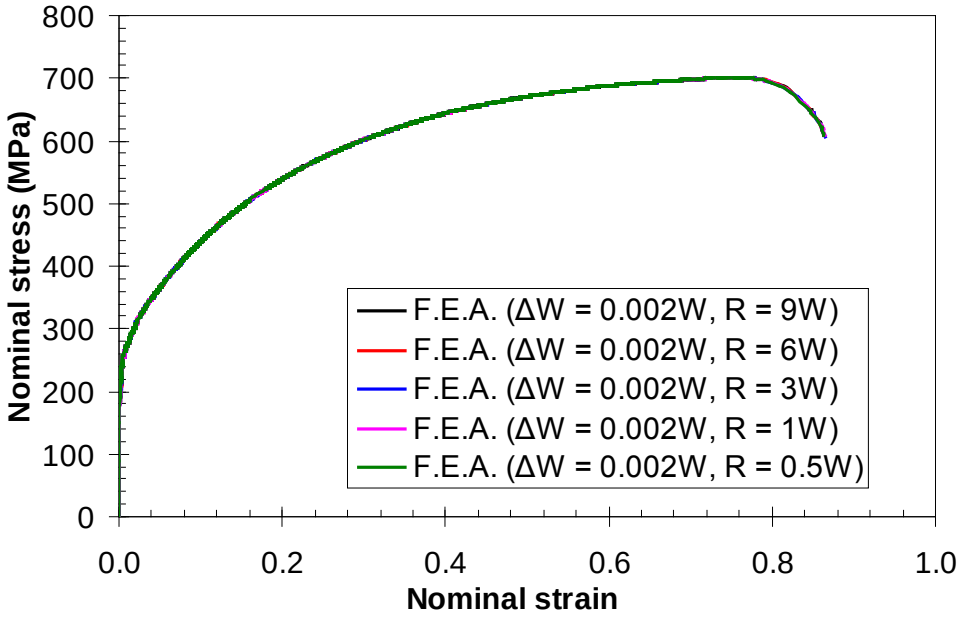

Fig. 8. Effect of the notch radius R on the predicted nominal stress-strain curve of flat specimen SB-304-LT.

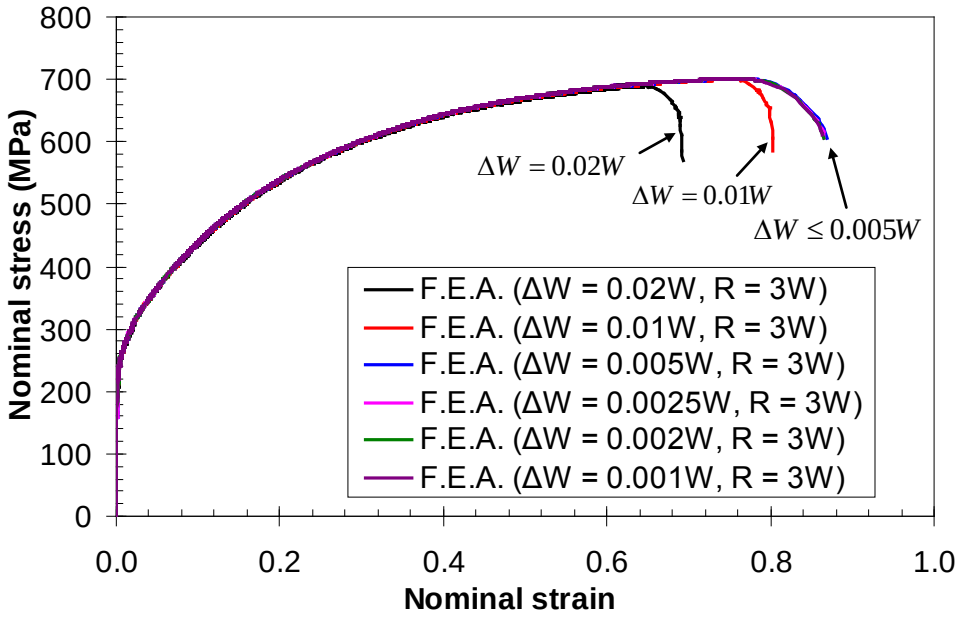

Fig. 9. Effect of ΔW on the predicted nominal stress-strain curve of flat specimen SB-304-LT.

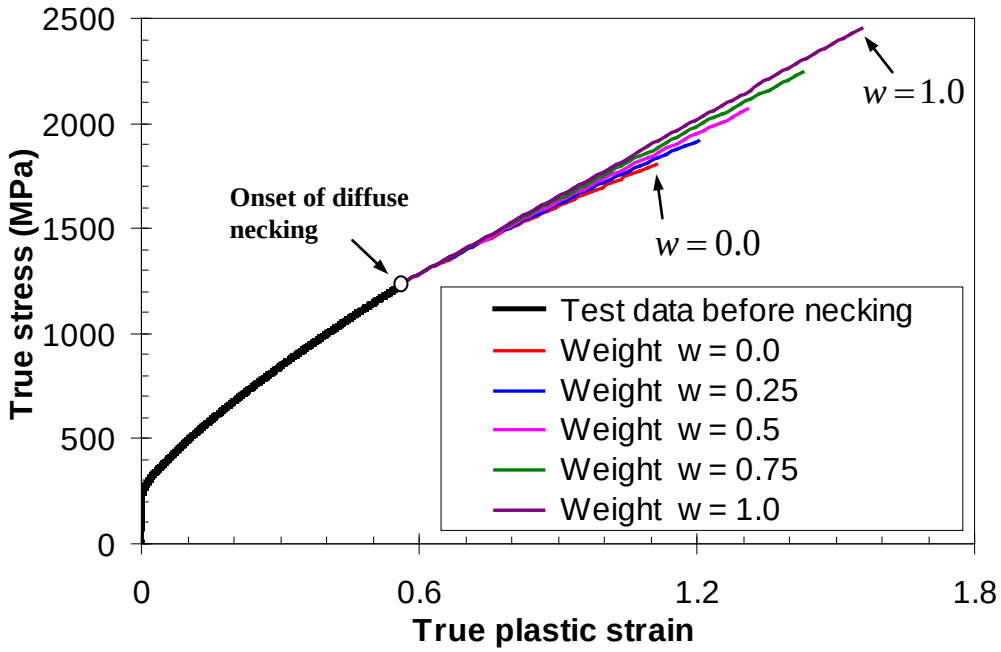

Fig. 10. Compound true stress-true plastic strain curves of flat specimen SB-304-LT for different trial weight constants.

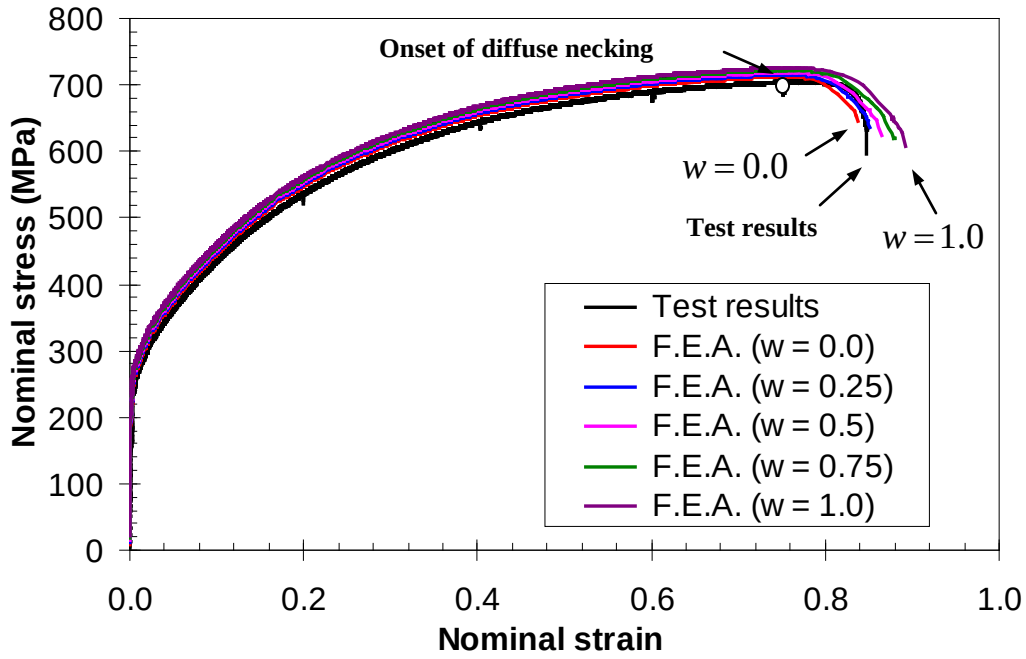

Fig. 11. Comparison between experimental and FE predicted nominal stress-strain curves of flat specimen SB-304-LT for different trial weight constants.

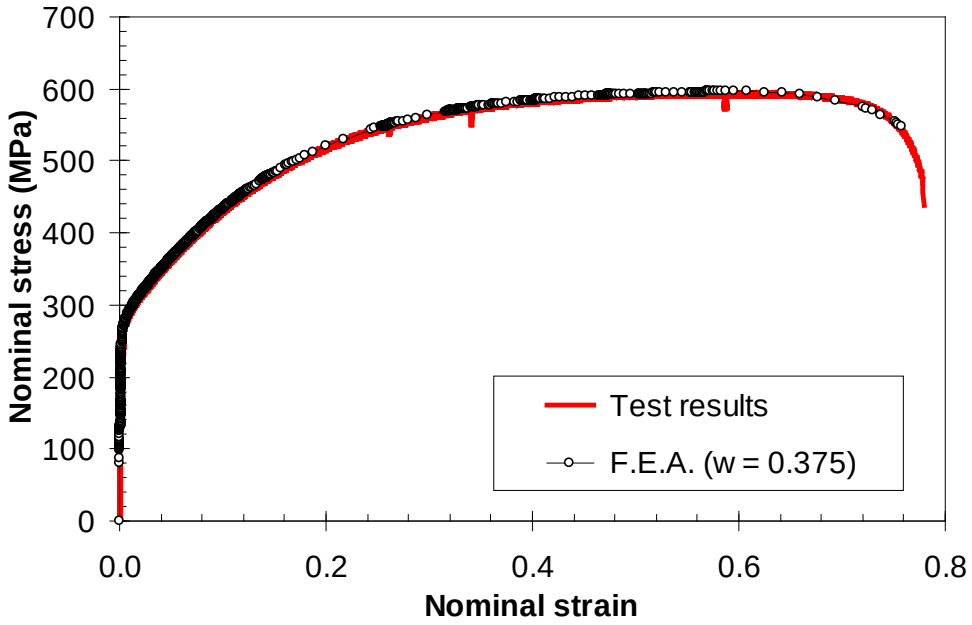

(a) Flat specimen FB-316L-LT (weight constant $w = 0.375$)

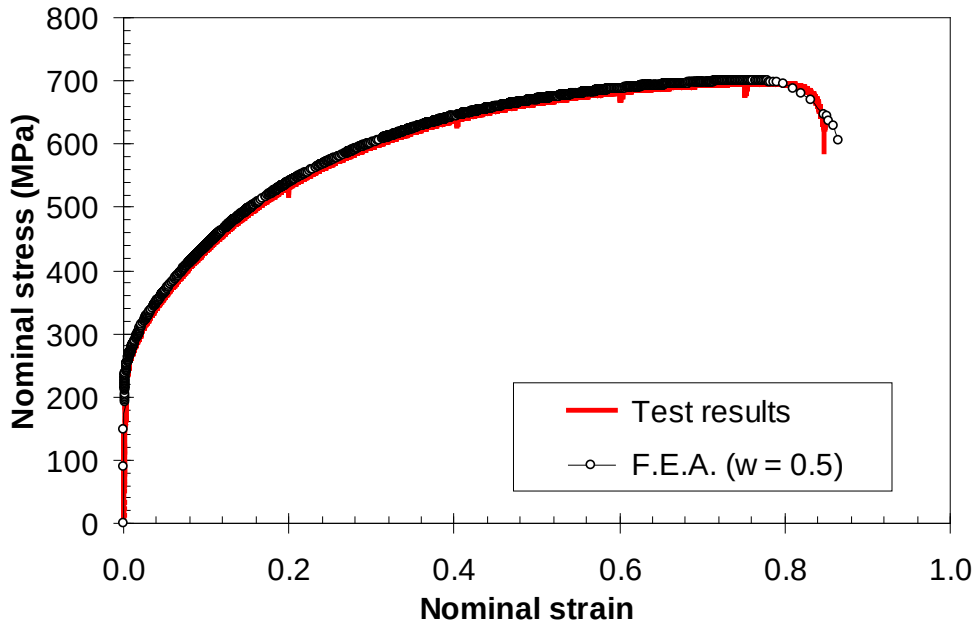

(b) Flat specimen SB-304-LT (weight constant $w = 0.5$)

Fig. 12. Comparisons between experimental and FE predicted stress-strain curves of flat specimens.

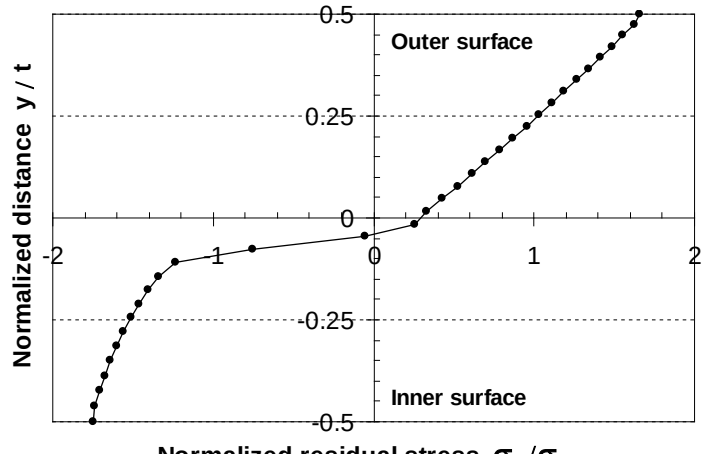

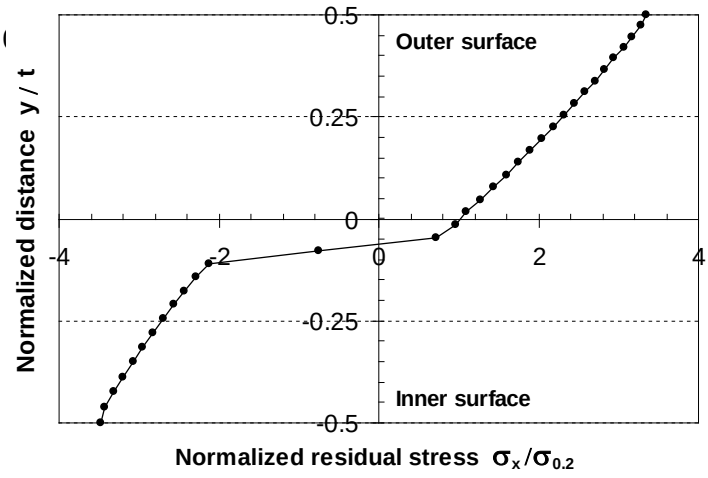

(b) Transverse residual stress

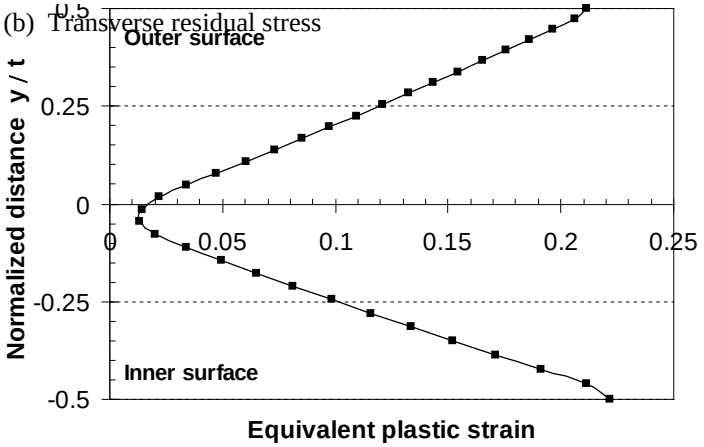

(c) Equivalent plastic strain

Fig. 13. FE predictions of residual stresses and equivalent plastic strains in corner specimen SB-304-SCr4t2 ($r_i / t = 2$).

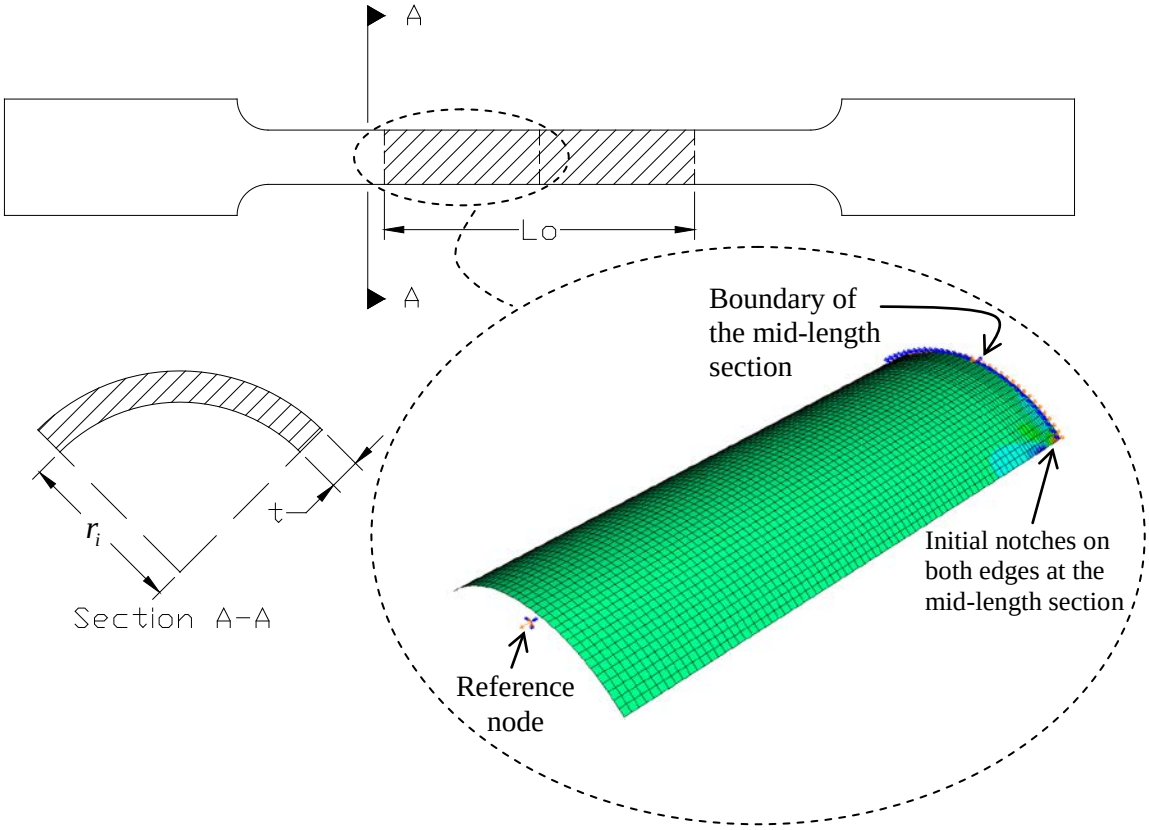

Fig. 14. Corner tension coupon and FE model.

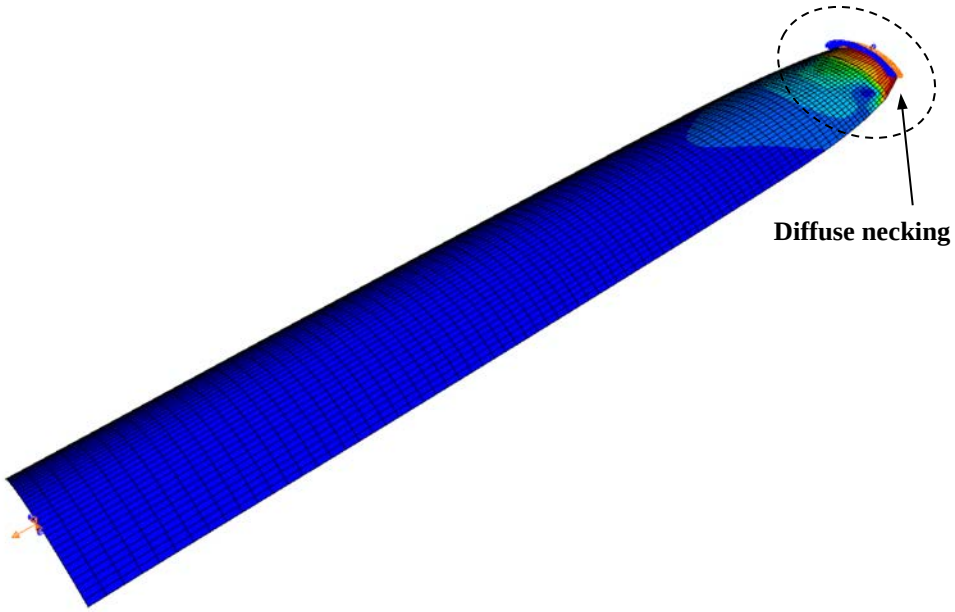

Fig. 15. Diffuse necking of a corner specimen in the FE simulation.

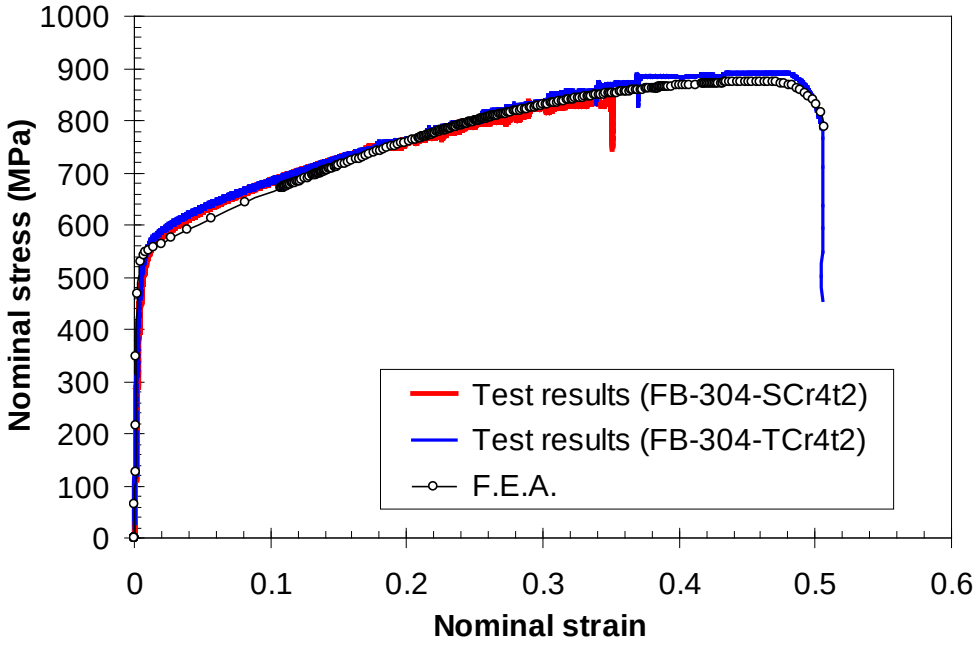

(a) Grade 304 and $r_i/t = 2$

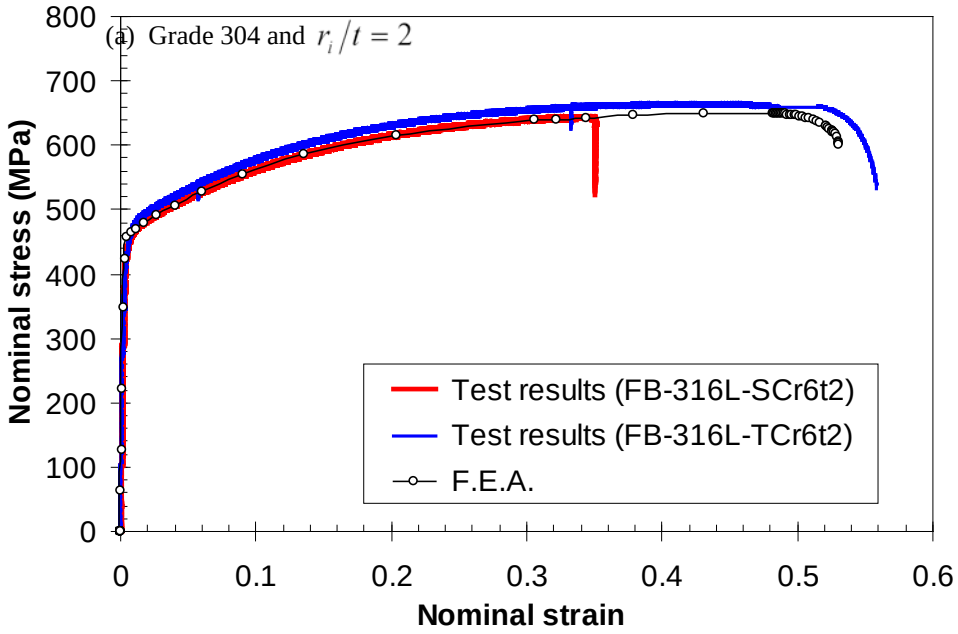

(b) Grade 316L and $r_i/t = 3$

Fig. 16. Comparisons between experimental and FE predicted stress-strain curves of corner specimens from the first batch.

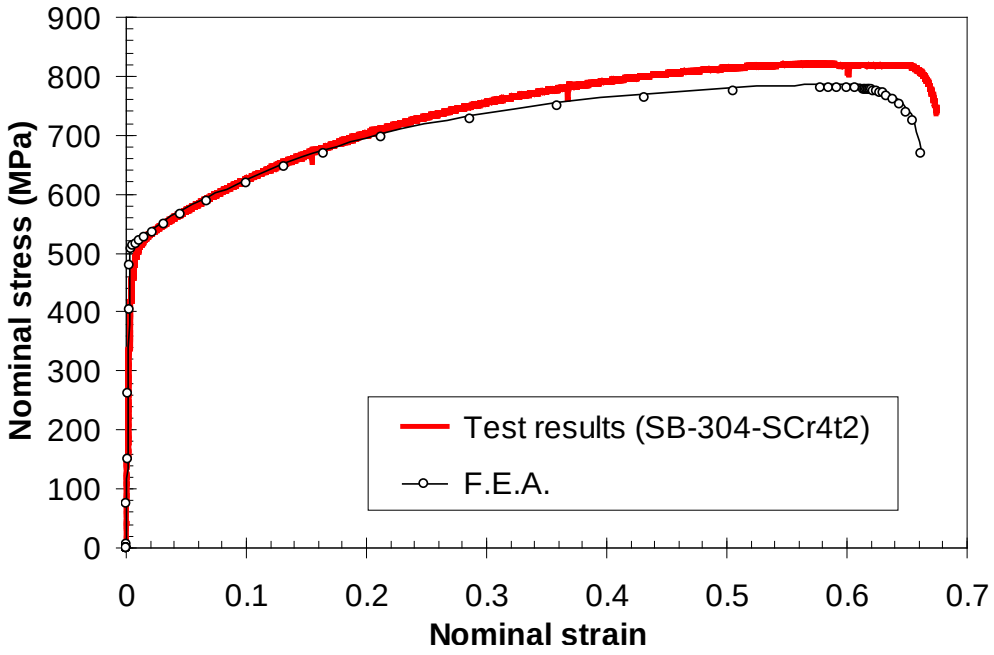

(a) Grade 304 and $r_i/t = 2$

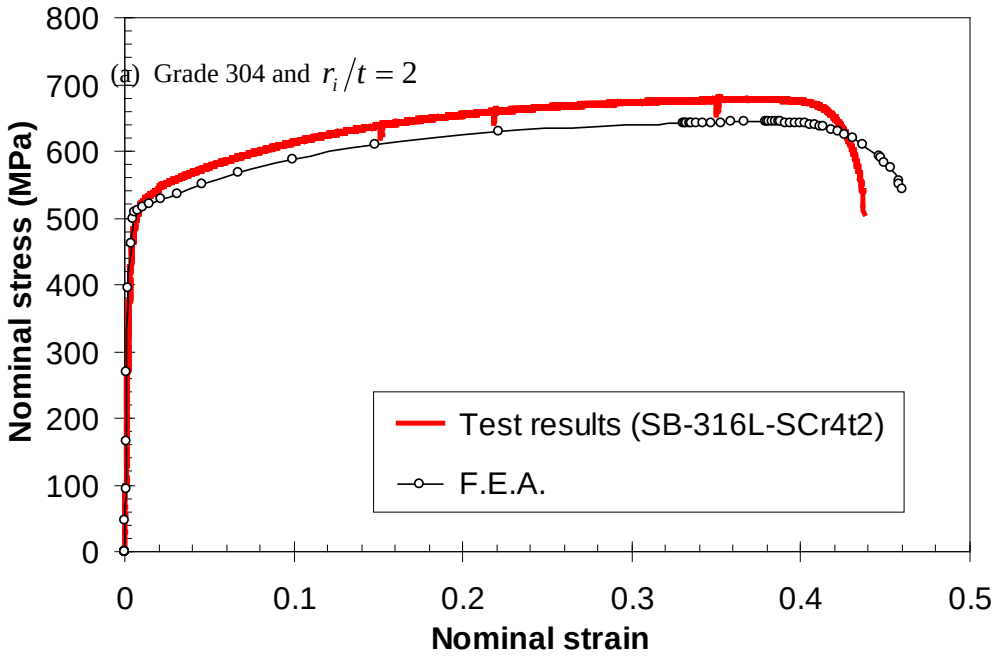

(b) Grade 316L and $r_i/t = 2$

Fig. 17. Comparisons between experimental and FE predicted stress-strain curves of corner specimens from the second batch.

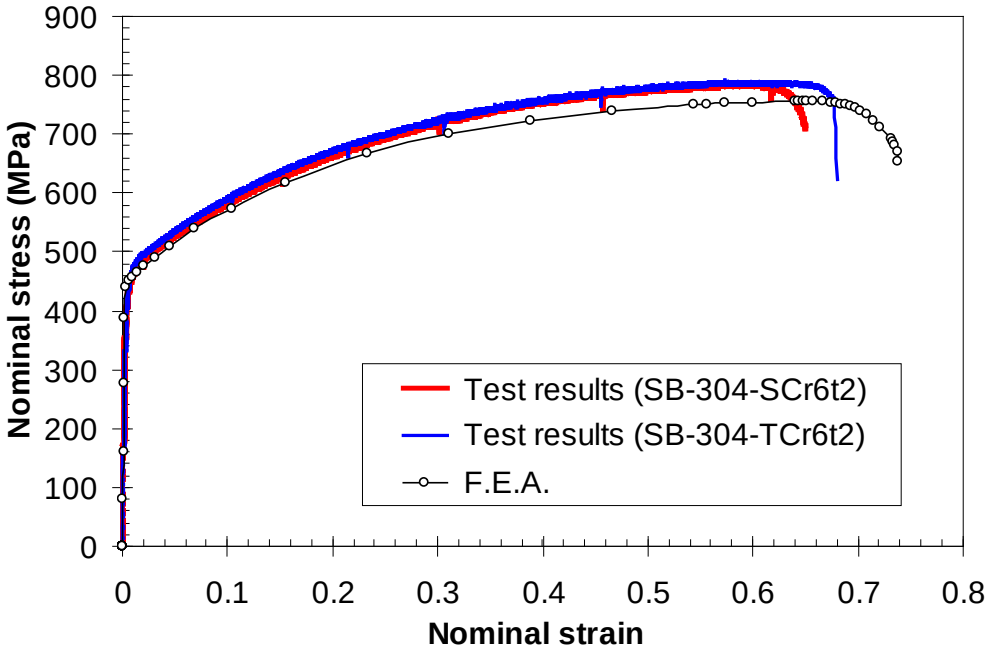

(a) Grade 304 and $r_i/t = 3$

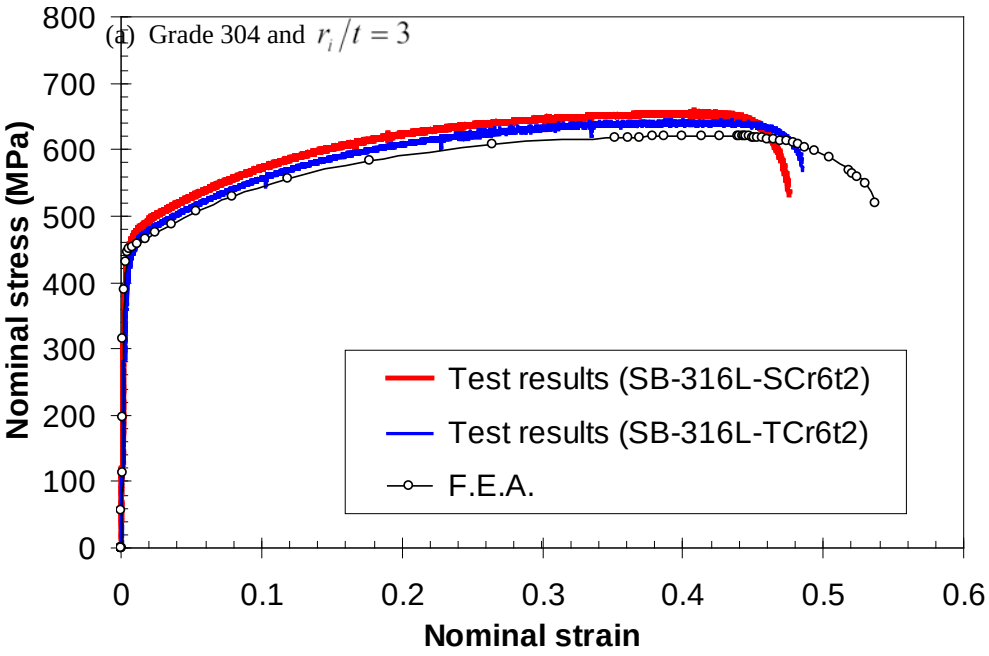

(d) Grade 316L and $r_i/t = 3$

Fig. 17. Comparisons between experimental and FE predicted stress-strain curves of corner specimens from the second batch (continued).